nature cell biology

AMBRA1 links autophagy to cell proliferation and tumorigenesis by promoting c-Myc dephosphorylation and degradation

Valentina Cianfanelli[1,2], Claudia Fuoco[3], Mar Lorente[4,5], Maria Salazar[4,5,13], Fabio Quondamatteo[6], Pier Federico Gherardini[3,13], Daniela De Zio[1], Francesca Nazio[2], Manuela Antonioli[3,7], Melania D'Orazio[3], Tatjana Skobo[8], Matteo Bordi[2], Mikkel Rohde[9], Luisa Dalla Valle[8], Manuela Helmer-Citterich[3], Christine Gretzmeier[10,11], Joern Dengjel[10,11], Gian Maria Fimia[7,12], Mauro Piacentini[3,7], Sabrina Di Bartolomeo[3], Guillermo Velasco[4,5] and Francesco Cecconi[1,2,3,14]

Inhibition of a main regulator of cell metabolism, the protein kinase mTOR, induces autophagy and inhibits cell proliferation. However, the molecular pathways involved in the cross-talk between these two mTOR-dependent cell processes are largely unknown. Here we show that the scaffold protein AMBRA1, a member of the autophagy signalling network and a downstream target of mTOR, regulates cell proliferation by facilitating the dephosphorylation and degradation of the proto-oncogene c-Myc. We found that AMBRA1 favours the interaction between c-Myc and its phosphatase PP2A and that, when mTOR is inhibited, it enhances PP2A activity on this specific target, thereby reducing the cell division rate. As expected, such a de-regulation of c-Myc correlates with increased tumorigenesis in AMBRA1-defective systems, thus supporting a role for *AMBRA1* as a haploinsufficient tumour suppressor gene.

As a response to nutrient deprivation and other cell stressors, autophagy is often induced in the context of reduced or arrested cell growth[1]. A plethora of signalling molecules and pathways have opposing effects on cell growth and autophagy, supporting the idea that these processes might represent mutually exclusive cell fates[2]. The serine/threonine kinase mTOR (mammalian target of rapamycin) integrates signals affecting both these pathways[3,4]. Indeed, mTOR has a major role in the regulation of protein synthesis, this in turn leading to cell growth inhibition, while also phosphorylating the pro-autophagic complex ULK1 and AMBRA1, resulting in the inhibition of autophagy[4–8]. Thus, autophagy inhibition by mTOR is known to occur independently of the mTOR targets related to cell growth[2].

A phosphatase known as a cell cycle regulator, the protein phosphatase 2A (PP2A), has been recently shown to also exert both a positive and negative effect on autophagy, depending on the particular step on which it acts and on its composition in subunits[9–11]. PP2A is usually a complex, containing a catalytic, a scaffold and a regulatory subunit. At least 100 different PP2A heterotrimeric complexes formed through combinatorial association of these subunits have been identified so far, thus mediating different specific physiological functions[12,13].

Recent studies have identified PP2A targets, whose dephosphorylation is critical for this phosphatase's tumour suppressor activity[14–16]: the transcription factor c-Myc is one such target. Inhibition of PP2A activity induces c-Myc Ser 62 (c-Myc^{S62}) phosphorylation and c-Myc protein stabilization, enhancing cell proliferation and impacting on tumorigenesis[17–19]. On growth-factor withdrawal, a massive dephosphorylation of c-Myc occurs, targeting the protein at the proteasome[19].
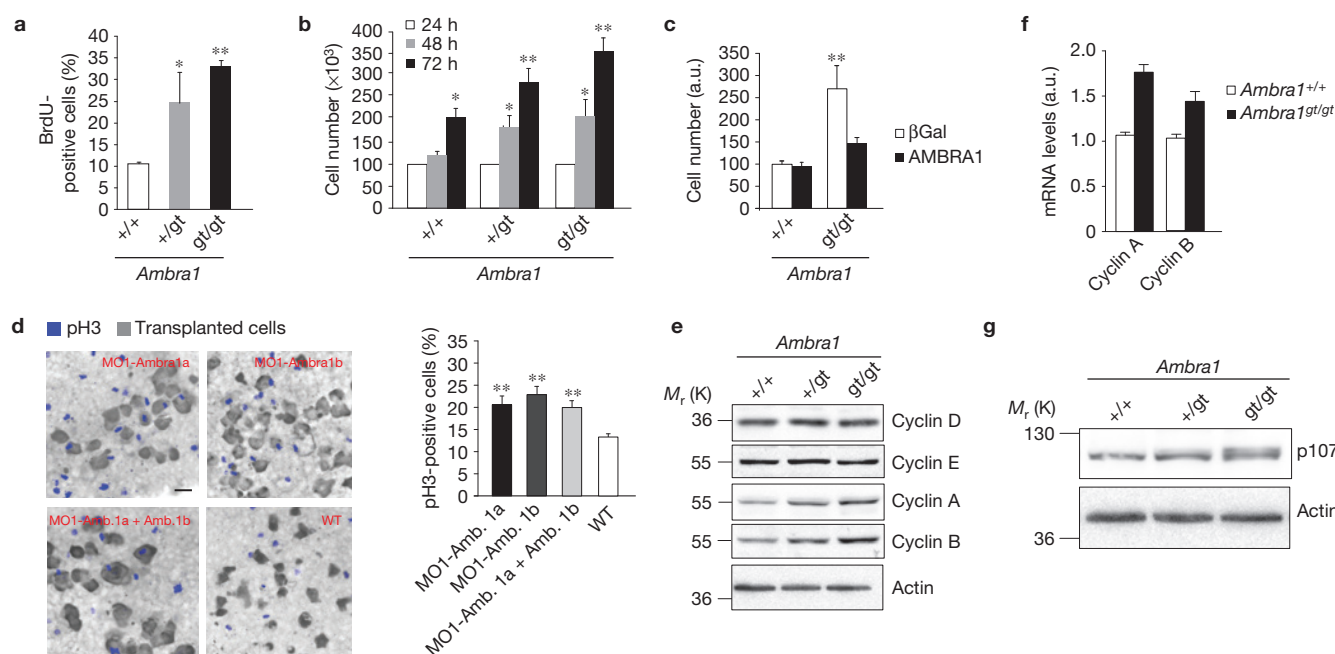
Figure 1 Ambra1 hemizygosity affects cell proliferation. (**a**) The proliferation rate of MEFs wild-type (+/+), heterozygous (+/gt) and homozygous (gt/gt) for the gene-trap mutation in the *Ambra1* locus was measured by BrdU-incorporation assay. Staining using anti-BrdU antibody was performed and BrdU-positive cells were counted. Data are presented as means ± s.d. and significance is *$P < 0.05$, **$P < 0.005$ ($n = 3$ independent experiments). (**b**) Cell counting of +/+, +/gt and gt/gt MEFs after 24, 48 and 72 h of growth. Data are presented as means ± s.d. and significance is *$P < 0.05$, **$P < 0.005$ ($n = 3$ independent experiments). (**c**) MEFs +/+ and gt/gt were immortalized through infection with RasV12 and E1A oncogenes. Subsequently, gene-trap MEFs were reconstituted for AMBRA1 by lentiviral infection; wild-type cells were infected with lentiviruses encoding for βGal, as a control. Data are presented as means ± s.d. and significance is **$P < 0.005$ ($n = 3$ independent experiments). (**d**) Zebrafish-embryo cells injected with morpholinos (MOs) against Ambra1 mRNA (MO1-Ambra1a, MO1-Ambra1b or both) were transplanted into wild-type embryos. The proliferation of the injected cells, reported in the graph, was calculated by counting pH3-positive cells (blue cells) with respect to the total implanted cells (grey cells). Scale bar, 20 μm. Data are presented as means ± s.d. and significance is **$P < 0.005$ ($n = 3$ independent experiments). (**e**) Protein extracts of +/+, +/gt and gt/gt MEFs were analysed by western blot, using antibodies against Cyclin D, E, A, B and Actin. (**f**) mRNA levels of Cyclin A and B were analysed by real-time PCR in MEFs +/+ and gt/gt. Data are presented as means ± s.e.m. ($n = 3$ independent experiments). (**g**) Electrophoretic mobility of p107 was analysed by western blot analysis in +/+, +/gt and gt/gt MEFs. An anti-p107 and an anti-Actin antibody were used. Uncropped images of blots are shown in Supplementary Fig. 7.

In this work, we characterize the pro-autophagic protein AMBRA1, a member of the autophagy signalling network in vertebrates[8,20,21], as an endogenous PP2A-interacting protein. In particular, on autophagy induction, AMBRA1 is phosphorylated by the kinase ULK1 and promotes autophagosome formation through the activation of the Class III PI(3)K complex[20,21]. Moreover, AMBRA1-mediated stabilization of ULK1 through regulative ubiquitylation enhances autophagy in a positive feedback loop[8].

In vivo inactivation of *Ambra1* gives rise to defects in the developing nervous system and results in embryonic death (*Ambra1$^{gt/gt}$* mice)[20,22]. In addition, an evident hyperproliferative phenotype has been associated with *Ambra1* depletion, both *in vitro* and *in vivo* even though the role of Ambra1 in cell cycle regulation remains completely unexplored[20,23]. Our results show that AMBRA1 enhances PP2A activity in c-Myc^{S62} dephosphorylation and thereby destabilizes c-Myc. Also, we demonstrate that *Ambra1* monoallelic deficiency is responsible for hyperproliferation, mainly dependent on the interaction with PP2A and on the stabilization of c-Myc. Moreover, this AMBRA1- and PP2A-mediated regulation of c-Myc is controlled by mTOR. As expected, such a de-regulation of the oncogene c-Myc correlates with increased tumorigenesis in AMBRA1-defective

systems, unravelling AMBRA1 as a haploinsufficient tumour suppressor gene.

RESULTS

Ambra1 dosage affects cell proliferation

To functionally characterize the role of AMBRA1 in cell proliferation, we generated mouse embryonic fibroblasts (MEFs) isolated from embryos wild-type (*Ambra1$^{+/+}$*), heterozygous (*Ambra1$^{+/gt}$*) or homozygous (*Ambra1$^{gt/gt}$*) for the gene-trap mutation in the *Ambra1* locus[20], and we evaluated the cell growth rate by bromodeoxyuridine (BrdU) staining and cell counting (Fig. 1a,b). We confirmed the hyperproliferative phenotype of *Ambra1$^{gt/gt}$* cells[20,23], and highlighted an increased proliferation rate in *Ambra1$^{+/gt}$* with respect to wild-type cells. Importantly, the Ambra1-depletion-elicited increase in cell growth is almost completely abolished by reconstitution of AMBRA1 levels in transformed (by RasV12/E1A expression) *Ambra1$^{gt/gt}$* MEFs, as demonstrated by an MTS assay (Fig. 1c). Moreover, the cell-autonomous capability of *Ambra1*-depleted cells to hyperproliferate is supported by the transplantation of zebrafish morphant *ambra1a* or *ambra1b* cells[23] in a wild-type acceptor embryo (Fig. 1d).
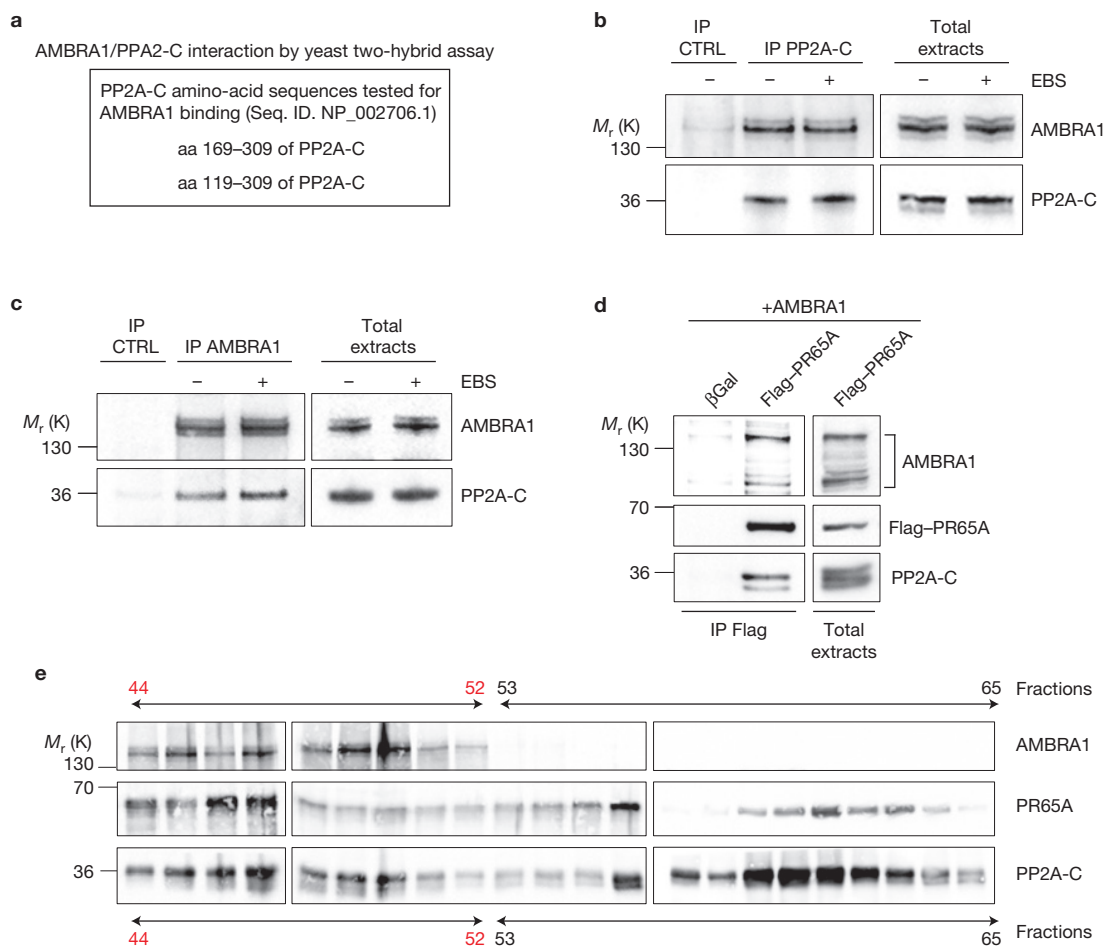
Figure 2 AMBRA1 is an interactor of PP2A (**a**) AMBRA1/PP2A-C interaction was identified by yeast two-hybrid assay. Yeast cells were co-transfected with a plasmid coding for AMBRA1 (ref. 20) and one coding for the reported regions of PP2A-C protein. The unities of βGal and the number of the clones positive for the screening are 5.7 and 4, respectively. (**b**) Endogenous protein extracts were immunoprecipitated using an anti-PP2A-C antibody (IP PP2A-C) and mouse immonuglobulins as control (IP CTRL). Purified complexes and corresponding total extracts were analysed by western blot using anti-AMBRA1 and anti-PP2A-C antibodies. EBS: Earle's balanced salts; an autophagy-inducer medium. (**c**) Endogenous protein extracts were immunoprecipitated using an anti-AMBRA1 antibody (IP AMBRA1) and rabbit immonuglobulins as control (IP CTRL). Purified complexes and corresponding total extracts were analysed as in **b**. (**d**) HEK293 cells were co-transfected with vectors encoding AMBRA1 and Flag–PR65A. Protein extracts were immunoprecipitated using an anti-Flag antibody. Purified complexes and corresponding total extracts were analysed by western blot using anti-AMBRA1, anti-Flag and anti-PP2A-C antibodies. The bracket indicates the bands corresponding to Flag–AMBRA1. (**e**) Protein extracts of HeLa cells were separated in different fractions and the presence of AMBRA1, PR65A and PP2A-C in the different fractions was assessed by western blot, using anti-AMBRA1, anti-PR65A and anti-PP2A-C antibodies. Uncropped images of blots are shown in Supplementary Fig. 7.

Further, the steady-state expression levels of some positive regulators of the cell cycle were evaluated in lysates from MEFs of different genotypes. All proteins analysed (Cyclin D, E, A and B) are responsible for the exit from the G^0 phase and for the transition from one to the subsequent phase of the cell cycle[24]. Unexpectedly, only Cyclin A and B were upregulated in Ambra1-defective MEFs (Fig. 1e), suggesting an enrichment in cells at S and M phase of the cell cycle[24]. Given that such upregulation could be due to transcriptional or post-translational control of Cyclins, we analysed Cyclin gene expression in $Ambra1^{+/+}$ and $Ambra1^{gt/gt}$ MEFs. As shown in Fig. 1f, the Cyclin A and B messenger RNAs are upregulated in Ambra1-deficient cells.

Primed by this result, we analysed the phosphorylation of a retinoblastoma family protein, p107, an event related to Cyclin A and B transcription, in Ambra1-defective MEFs. A p107 band with lower electrophoresis mobility appears in $Ambra1^{gt/gt}$ MEFs (Fig. 1g), suggesting that Ambra1 may be important for the dephosphorylation of p107 (ref. 25). Intriguingly, p107 has been identified as a target of the phosphatase PP2A, involved in autophagy regulation[9,10,26].

To summarize, these analyses demonstrate that the loss of a single $Ambra1$ allele is sufficient to increase cell proliferation and that this hyperproliferative phenotype correlates with increased transcription of Cyclin A and B and inactivation of their transcriptional inhibitor p107.

AMBRA1 is an interactor of PP2A

We identified the catalytic subunit of PP2A as an AMBRA1 interactor by both yeast two-hybrid and tandem affinity purification approaches (Fig. 2a and Supplementary Table 1). To verify this interaction,
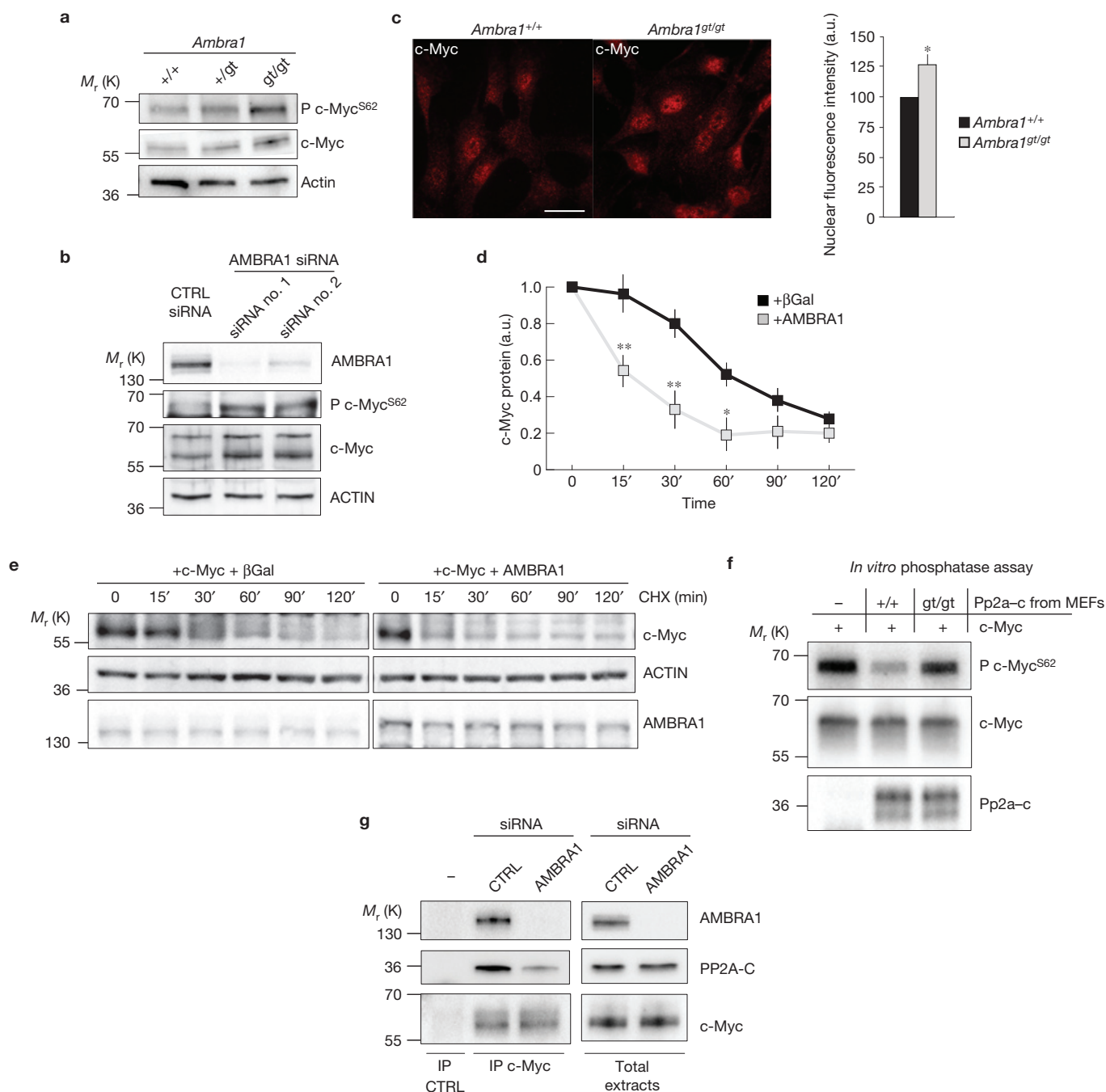
Figure 3 AMBRA1 affects c-Myc dephosphorylation at Ser 62. (**a**) Protein extracts of MEFs wild-type (+/+), heterozygous (+/gt) and homozygous (gt/gt) for the gene-trap mutation in the *Ambra1* locus were analysed by western blot, using antibodies against c-Myc phosphorylated at the Ser 62 (P c-Myc[S62]), total c-Myc and Actin. (**b**) Protein extracts of HeLa cells knocked down for AMBRA1 (siRNA no. 1 and no. 2) or treated with aspecific oligonucleotides (CTRL siRNA), as a control, were analysed by western blot, using antibodies against P c-Myc[S62], total c-Myc and ACTIN. (**c**) Immunostaining of c-Myc in +/+ and gt/gt MEFs. Scale bar, 20 μm. Fluorescence intensity per cell was quantified by ImageJ software, as previously described[53]. Data are presented as means ± s.e.m. and significance is *$P < 0.05$ ($n = 100$ cells pooled from 3 independent experiments in which 6–8 fields were assessed per experiment). (**d,e**) Cells co-transfected with c-Myc and AMBRA1 or βGal, as a control, were treated with cycloheximide (CHX) and collected at the indicated time points. Protein extracts of cells were analysed by western blot, using antibodies against c-Myc, AMBRA1 and ACTIN. Quantification is shown in **d**. Data are presented as mean ± s.d. and significance is *$P < 0.5$ and **$P < 0.05$ ($n = 3$ independent experiments). (**f**) Different phosphatase reactions were performed *in vitro*, using Pp2a-c extracted from +/+ or gt/gt cells, incubated with the same amount of c-Myc. c-Myc immunoprecipitation plus mouse immunoglobulin mix, instead of anti-Pp2a-c, was used as a negative control. The products of the reactions were analysed by western blot, using antibodies against P c-Myc[S62], total c-Myc and Pp2a-c. (**g**) HeLa cells were knocked down for AMBRA1 (AMBRA1 siRNA) or treated with aspecific oligonucleotides (CTRL siRNA), as a control. Endogenous c-Myc was immunoprecipitated using an anti-c-Myc antibody (IP c-Myc) and mouse immunoglobulins were used as a control (IP CTRL). The immunoprecipitated complexes were analysed by western blot with anti-AMBRA1, anti-c-Myc and anti-PP2A-C antibodies. Uncropped images of blots are shown in Supplementary Fig. 7.

co-immunoprecipitation analyses were performed from endogenous extracts of HeLa cells (Fig. 2b,c). We found that, independently of autophagy modulation, endogenous PP2A-C interacts with AMBRA1. To map the AMBRA1/PP2A-C interaction we tested a number of AMBRA1 constructs for their capacity to co-immunoprecipitate with PP2A-C. Only fragments corresponding to amino acids 181–532 and 946–1269 were able to bind PP2A-C (regions F1WD40 and F3b, Supplementary Fig. 1). Of note, even though the regulative B-subunits of PP2A are usually characterized by WD40 domains, allowing both their association to the PP2A complex and the substrate recognition[12,13], the AMBRA1 regions here identified contain no WD40 domains (otherwise present at its amino terminus).

As mentioned above, the catalytic subunit of PP2A (PP2A-C), together with the regulatory (B subunit) and the scaffold (PR65A) subunits, constitutes a holoenzyme that also other PP2A-C interactors can join[12,13]. Indeed, AMBRA1 can also interact with PR65A along with PP2A-C (Fig. 2d and Supplementary Fig. 2a,b), and the three proteins are in a high-molecular-weight multimeric complex (Fig. 2e, fractions 44–53, in red). As expected, heterodimers of PP2A-C and PR65A can also associate in the absence of AMBRA1 (Fig. 2e, fractions 53–63).

AMBRA1 promotes PP2A activity on c-Myc

PP2A-C is known to bind scaffold proteins or different regulatory subunits that mediate specific substrate docking[15]. This evidence, together with our findings concerning the roles of AMBRA1 and its interaction with PP2A-C, suggests that AMBRA1 may regulate PP2A activity on some substrates, thus controlling cell proliferation.

To verify this hypothesis, and given the effect of Ambra1 depletion on the PP2A substrate p107 (ref. 26), we also analysed the phosphorylation level of c-Myc, identified as another crucial target of PP2A (ref. 18).

Interestingly, we found that Ambra1 depletion in MEFs or AMBRA1 downregulation in HeLa cells increases c-Myc^{S62} phosphorylation (P c-Myc^{S62}) relative to total c-Myc (Fig. 3a,b). In addition, a slight increase in the levels of total c-Myc is observed in cells devoid of Ambra1 (Fig. 3a,b and Supplementary Fig. 2c,d), probably as a consequence of c-Myc stabilization through Ser 62 phosphorylation; further, the c-Myc nuclear fraction (functional in controlling cell proliferation) is also increased in Ambra1-depleted cells (Fig. 3c). In contrast, no marked differences were observed in the expression or phosphorylation of other known targets of PP2A-C (Supplementary Fig. 3a,b)[15], arguing for high specificity of the role of AMBRA1 in this regulation. Also, we ruled out the possible involvement of the c-Myc protein kinases[17] in the observed de-regulation of c-Myc on Ambra1 depletion, by analysing Erk1/2 phosphorylation levels (Supplementary Fig. 3b). Finally, increased AMBRA1 levels are able to induce a diminished half-life of total c-Myc (Fig. 3d,e). Taken together, these results demonstrate that AMBRA1 promotes c-Myc dephosphorylation and destabilization. Primed by these findings, we set out to establish, by means of an *in vitro* phosphatase assay, whether AMBRA1 enhanced PP2A-C activity on c-Myc. To this end, c-Myc immunoprecipitates from P c-Myc^{S62}-enriched cells were incubated with independent pools of Pp2a-c isolated from wild-type ($Ambra1^{+/+}$) or Ambra1-deficient ($Ambra1^{gt/gt}$) MEFs (Fig. 3f). Interestingly, Ambra1 depletion clearly decreased PP2A-C activity on P c-Myc^{S62}.

Next, we found that endogenous c-Myc is in the same complex with AMBRA1 and PP2A-C and that AMBRA1 depletion by transient knockdown affects the interaction between c-Myc and PP2A-C (Fig. 3g).

Taken together, these experiments provide biochemical evidence that AMBRA1 favours the recruitment of PP2A to c-Myc and enhances c-Myc-associated PP2A activity. This decreases P c-Myc^{S62} and results in the de-stabilization of the protein.

mTOR is upstream of AMBRA1 in controlling c-Myc

Although mTOR is considered a key regulator of both cell growth and autophagy[2,3], the mTOR target molecules in this co-regulation have not yet been identified. We have shown that mTOR-mediated phosphorylation on AMBRA1 results in the negative regulation of autophagy[8]. Thus, we verified whether mTOR could also affect AMBRA1/PP2A-C-mediated dephosphorylation of c-Myc. We found c-Myc to be dephosphorylated at Ser 62 on mTOR inhibition by both rapamycin and Torin1 treatments and by amino-acid starvation (Fig. 4a–c); we also verified the involvement of mTOR in the regulation of c-Myc by targeting RAPTOR, a component of the mTORC1 complex, whose depletion results in mTOR inhibition[25]. As expected, also in this case, c-Myc dephosphorylation on Ser 62 was observed (Fig. 4d). In contrast, cells lacking the mTORC1 inhibitor Tsc2 (ref. 27) are characterized by high levels of P c-Myc^{S62} (Fig. 4e). In line with the role of c-Myc^{S62} phosphorylation in this protein stability, a decrease of total c-Myc is also observed on prolonged mTOR inhibition (Fig. 4f–h). Further, by depleting AMBRA1 on mTOR negative regulation, we also found that AMBRA1 is required to maintain the inhibitory effect of mTOR on c-Myc (Fig. 4i–k).

AMBRA1 controls cell proliferation by c-Myc regulation

To verify the impact of the AMBRA1/PP2A/c-Myc interaction on cell cycle regulation, we generated a mutant AMBRA1 incapable of binding PP2A-C. In order not to affect AMBRA1 interaction with its additional binding partners, we used a site-specific mutation approach. AMBRA1 is an intrinsically disordered protein[28], having no domains but the WD40s. For this reason, we considered the presence of a linear motif in the AMBRA1 sequence to be responsible for binding PP2A-C. By analysing the amino-acid sequences of both regions previously identified as responsible for PP2A-C interaction (F1ΔWD40 and F3b, respectively; Supplementary Fig. 1), and as independently capable of binding PP2A-C, we identified a single conserved peptide with the sequence PQPSTxR. The motif PxPxxxR is reminiscent of SH3-binding motifs, which consist of a PxxP core with a positively charged residue either preceding or following this consensus[29] and already shown as relevant for PP2A binding[30]. We thus mutated both potential binding sites on AMBRA1 (AMBRA1^{PXP}) (Fig. 5a and Supplementary Fig. 2a,b), and so disrupted AMBRA1/PP2A-C interaction, whereas mutagenesis of each single motif (AMBRA1^{NT-PXP}, AMBRA1^{CT-PXP}) did not (Supplementary Figs 2a,b and 4a,b).

Next, we used AMBRA1^{PXP} to assess its effect on AMBRA1-mediated regulation of c-Myc and on cell proliferation. As expected, the expression of AMBRA1^{PXP} in AMBRA1-deficient cells does not restore normal P c-Myc^{S62} levels (Fig. 5b,c), and has no effect on cell numbers (Fig. 5d), at a variance with AMBRA1^{WT}.
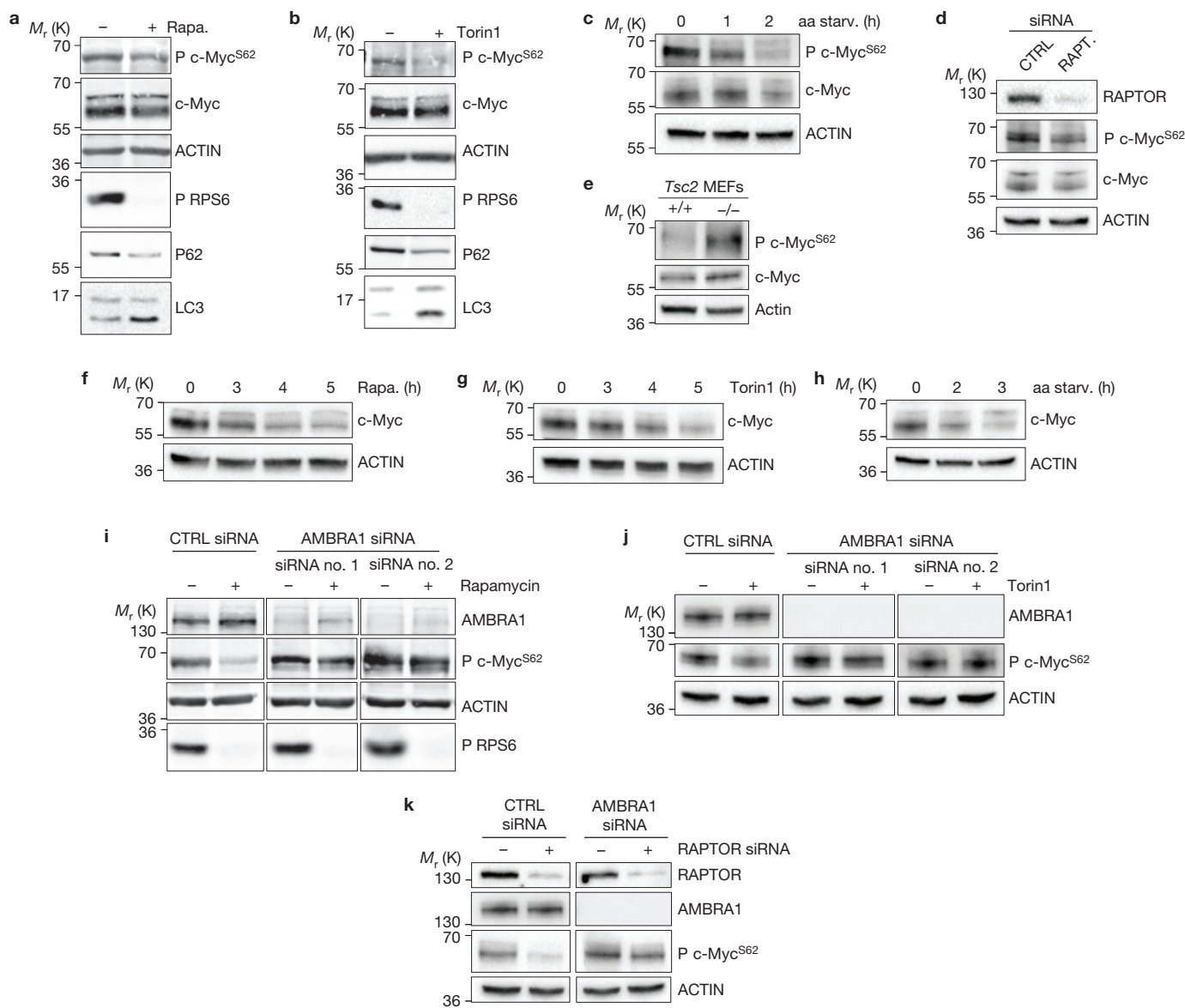
Figure 4 Inhibition of mTOR affects c-Myc phosphorylation at Ser 62 in an AMBRA1-dependent manner. (**a**) HeLa cells were treated with rapamycin for 2 h and protein extracts were analysed by western blot using antibodies against P c-Myc^{S62}, total c-Myc, ACTIN, phospho-RPS6, p62 and LC3. (**b**) HeLa cells were treated with Torin1 for 2 h and protein extracts were analysed by western blot using the same antibodies as in **a**. (**c**) The levels of P c-Myc^{S62} were measured in HeLa cells on amino-acid starvation (aa starv.); protein extracts were analysed by western blot using antibodies against P c-Myc^{S62}, total c-Myc and ACTIN. (**d**) Protein extracts of HeLa cells knocked down for RAPTOR (RAPT.) or treated with aspecific oligonucleotides (CTRL), as a control, were analysed by western blot, using the anti-RAPTOR antibody and the same antibodies as in **c**. (**e**) Protein extracts of immortalized MEFs, wild-type (+/+) and knock-out (−/−) for *Tsc2*, were analysed by western blot, using the same antibodies as in **c**. (**f**) HeLa cells were treated with rapamycin for 3 h, 4 h and 5 h. Protein extracts were analysed by western blot using the antibodies against total c-Myc and ACTIN. (**g**) HeLa cells were treated with Torin1 for 3 h, 4 h and 5 h. Protein extracts were analysed by western blot using the same antibodies as in **f**. (**h**) HeLa cells were amino-acid-starved and protein extracts were analysed by western blot using the same antibodies as in **f**. (**i**) HeLa cells treated with oligo-interference against AMBRA1 (siRNA no. 1 and no. 2) or with aspecific oligonucleotides (CTRL siRNA) were incubated with rapamycin for 2 h. Protein extracts were analysed by western blot using anti-AMBRA1, anti-P c-Myc^{S62}, ACTIN and phospho-RPS6 antibodies. (**j**) HeLa cells treated as in **i** were incubated with Torin1 for 2 h. Protein extracts were analysed by western blot using antibodies against AMBRA1, P c-Myc^{S62} and ACTIN. (**k**) HeLa cells were first treated with oligo-interference against AMBRA1 (AMBRA1 siRNA) and, after 24 h, with oligonucleotides against RAPTOR (+RAPTOR siRNA). For each transfection, suitable aspecific oligonucleotides (CTRL siRNA; −RAPTOR siRNA) were used. Protein extracts were analysed by western blot using antibodies against RAPTOR, AMBRA1, P c-Myc^{S62} and ACTIN. Uncropped images of blots are shown in Supplementary Fig. 7.

In contrast, no difference can be observed in the pro-autophagic capability of the mutant AMBRA1^{PXP} when compared with the wild-type (AMBRA1^{WT}) (Supplementary Figs 2a,b and 4c) and, indeed, AMBRA1^{PXP} can still bind both BECLIN 1 and ULK1, two AMBRA1 interactors in the autophagy pathway[8,20,21] (Supplementary Figs 2a,b and 4d,e).
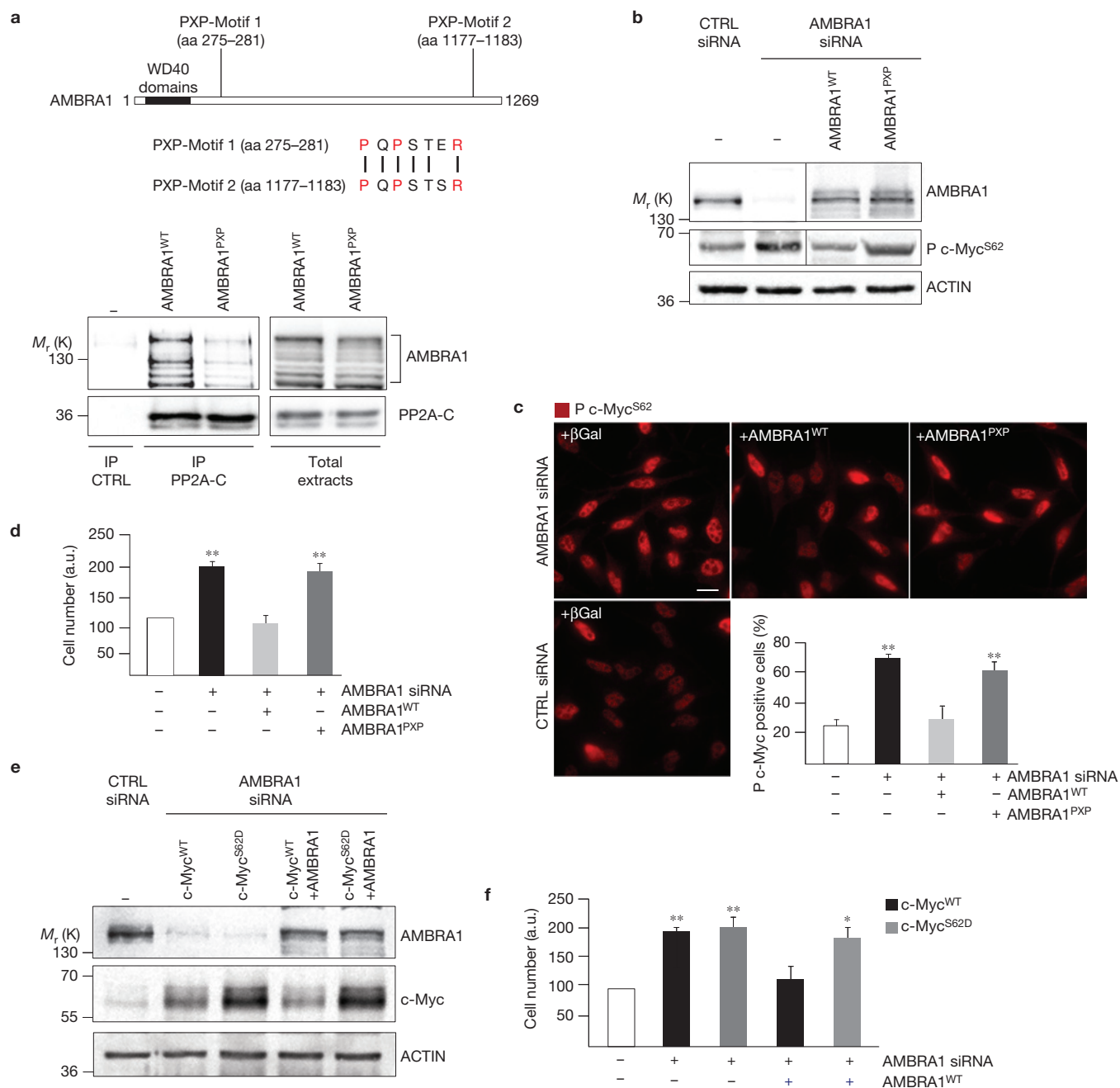
Figure 5 AMBRA1 affects c-Myc phosphorylation and cell proliferation through its direct binding to PP2A-C. (**a**) HEK293 cells were transfected with AMBRA1 or AMBRA1^{PXP}. Protein extracts were used for PP2A-C immunoprecipitation and the immunocomplexes were analysed by western blot, with anti-AMBRA1 and anti-PP2A-C antibodies. A schematic representation of PXP motifs on AMBRA1 and ClustalW alignment of the two motifs present in AMBRA1 (corresponding to amino acids 275–281 and 1177–1183) are reported. (**b**) HeLa cells knocked down for AMBRA1 (or with unrelated control siRNA, −) and reconstituted with AMBRA1^{WT}, with AMBRA1^{PXP} or with βGal, as a control, were analysed for the amount of P c-Myc^{S62} by western blot. In addition, an antibody against AMBRA1 was used to check for successful AMBRA1 knockdown and reconstitution. Anti-ACTIN antibody was used as a loading control. The vertical line represents a splice mark. The samples were obtained and processed in the same experiment, and the gels/blots were processed in parallel. (**c**) HeLa cells, transfected as in **b**, were analysed for the localization and amount of P c-Myc^{S62}. P c-Myc^{S62}-positive cells were counted. Data are presented as means ± s.d. and significance is **$P < 0.005$ ($n = 100$ cells pooled from 3 independent experiments in which 6–8 fields were assessed per experiment). Scale bar, 10 μm. (**d**) HeLa cells knocked down for endogenous AMBRA1 and reconstituted with AMBRA1^{WT} or with AMBRA1^{PXP} were analysed by MTS assay. Data are presented as means ± s.d. and significance is **$P < 0.005$ ($n = 3$ independent experiments). (**e**) HeLa cells were knocked down for AMBRA1 (or with unrelated control siRNA, CTRL) and transfected with wild-type c-Myc (c-Myc^{WT}) or phosphomimicking c-Myc (c-Myc^{S62D}). Subsequently, cells were reconstituted with AMBRA1^{WT} or transfected with βGal, as a control. In these cells, we analysed the amount of c-Myc and AMBRA1 by western blot, to check for AMBRA1 knockdown/transfection and for c-Myc transfection. Anti-ACTIN antibody was used as a loading control. (**f**) Cells treated as in **e** were analysed by MTS assay (see **d**). Data are presented as means ± s.d. and significance is *$P < 0.05$, **$P < 0.005$ ($n = 3$ independent experiments). Uncropped images of blots are shown in Supplementary Fig. 7.

Last, we verified the significance of c-Myc dephosphorylation in this AMBRA1-dependent regulation. On c-Myc constitutive phosphorylation (by means of the phosphomimicking c-Myc^{S62D} mutant construct) and by co-transfecting AMBRA1 in AMBRA1 knocked down cells, we could not compensate for the AMBRA1-deficient phenotype, in contrast to what we observe with wild-type c-Myc (Fig. 5e,f). This finding implies that c-Myc dephosphorylation is, indeed, absolutely required for this pathway of regulation. In line with the role of AMBRA1 in the regulation of c-Myc stability, in this experiment we also observed a decrease of exogenous total c-Myc^{WT} on AMBRA1 overexpression (Fig. 5e).

Ambra1 is a tumour suppressor gene

Given the effect of Ambra1 on cell proliferation and on c-Myc stability, we set out to assess whether *Ambra1* could be considered as a tumour suppressor gene *in vivo*. We addressed this issue by subcutaneously injecting into athymic mice primary MEFs, wild-type (*Ambra1$^{+/+}$*) and null (*Ambra1$^{gt/gt}$*) for the *Ambra1* locus, transformed by a lentivirus encoding two oncogenes, a constitutively active form of Ras (RasV12) and E1A. Mice xenografted with MEFs devoid of *Ambra1* (*Ambra1$^{gt/gt}$*) or expressing AMBRA1 mutated in the PP2A-binding sites (*Ambra1$^{gt/gt}$ + AMBRA1^{PXP}*) developed tumours earlier compared with the animals injected with the *Ambra1$^{+/+}$* cells or the *Ambra1$^{gt/gt}$* reconstituted with wild-type AMBRA1 (*Ambra1$^{gt/gt}$ + AMBRA1^{WT}*) (Fig. 6a).

Also, an increase in P c-Myc^{S62} and, to a lesser extent, in total c-Myc, characterizes *Ambra1*-defective tumours (Fig. 6b), together with a higher number of proliferating cells (Fig. 6c).

We then analysed whether *Ambra1* allelic dosage and expression levels (Supplementary Fig. 5a,b) were responsible for spontaneous tumour insurgence in wild-type and *Ambra1$^{+/gt}$* mice between 12 and 17 months of age. Indeed, as shown in Fig. 6d, a monoallelic deletion of *Ambra1* is considered sufficient to increase the occurrence of tumours that primarily affected liver and lungs, the latter with areas of pulmonary parenchyma, in which the spongy organization typical of the alveoli was no longer recognizable and the tissue had a solid appearance (Fig. 6e, left panels). These lesions appear as circumscribed round masses, with a papillary architecture and glandular aspects, in the absence of a well-structured fibrous capsule, suggesting tumour aggressiveness (Fig. 6f); in fact, they express the thyroid transcription factor-1 (TTF-1; ref. 31), a *bona fide* marker of lung carcinomas, normally expressed also in bronchial and type II alveolar epithelial cells of the healthy tissue (Fig. 6e, middle/right panels). Also, the presence of Ambra1 in the *Ambra1$^{+/gt}$* tumours demonstrates that they are not characterized by loss of heterozygosity (Supplementary Fig. 5c). Indeed, Ambra1 levels seem to be augmented in the hemizygous samples, most likely owing to a feedback attempt of the cells to enhance the activity of their autophagy machinery. Last, *Ambra1$^{+/gt}$* apparently healthy bronchioli show a high positivity to Ki-67, a cell proliferation marker, whereas cell proliferation is usually extremely low in normal (wild-type) lung epithelia, with only ≈0.5% of airway cells actively dividing[32–34] (Fig. 6g, immunohistochemistry upper panels). However, tumour-bearing lung sections also show a focal positivity to the proliferation marker (Fig. 6g, immunohistochemistry lower panels), suggesting that tumour growth is also sustained by cell proliferation. In the light of the role of Ambra1 in the positive regulation of autophagy, we monitored the autophagy levels in Ambra1-deficient tumours. An inhibition of the autophagy pathway was found, as expected, in *Ambra1$^{+/gt}$* tumours, as proved by analysis of the autophagy marker p62 (Supplementary Fig. 5d,e). This is in line with what was reported on inactivation of other autophagy regulators[35–39].

Importantly, we also found AMBRA1 mutations in human tumours (in the endometrium, large intestine and urinary tract, with 2.2%, 2.9% and 2.94% frequency of mutation, respectively) and a clear inverse correlation between AMBRA1 and P c-Myc^{S62} levels in a number of lung adenocarcinoma cell lines and a breast carcinoma cell line (Fig. 6g,h and Supplementary Figs 2e and 6). Interestingly, when overexpressing AMBRA1 in cancer cell lines characterized by the lowest endogenous AMBRA1 levels, we were able to decrease c-Myc^{S62} phosphorylation (right panels in Fig. 6h,i, and Supplementary Figs 2a,b and 6a,b), whereas, in the same cell lines, AMBRA1 overexpression induced lower proliferation and decreased tumorigenicity (Fig. 6j,k and Supplementary Fig. 6c,d). On the basis of our results, we thus demonstrate that disruption of the *Ambra1* locus is sufficient to induce c-Myc hyperphosphorylation, hyperproliferation and tumorigenesis.

DISCUSSION

We previously demonstrated that the upstream autophagy regulator AMBRA1 (refs 8,20,21) affects cell proliferation both *in vitro* and *in vivo*[20,23]. In this study we show that this role may be based on the mTOR-controlled AMBRA1 regulation of the phosphatase PP2A towards its substrate c-Myc, impacting cell proliferation and tumorigenesis.

Notably, protein–protein interactions between PP2A and cellular scaffolds other than its canonical subunits contribute to the specificity of PP2A signalling[40]. In this scenario, at least two possible roles for AMBRA1 can be considered: AMBRA1 could be either a regulatory subunit of the complex or a member of the heterotrimeric complex, formed by PP2A-C, PR65A and a regulatory subunit that we have yet to identify. As a PP2A interactor, we found that AMBRA1 may facilitate c-Myc dephosphorylation in a specific manner, because other PP2A substrates were unaffected by AMBRA1 dosage. On the other hand, we also found a hyperphosphorylation of the transcription factor p107, another PP2A substrate[26], in Ambra1-defective systems. However, the dephosphorylation of p107 is carried out by both PP2A and the phosphatase PP1 (ref. 41), although it is difficult to distinguish the two activities, because specific antibodies for the different phosphorylation sites of the two phosphatases are not available.

As for the biochemistry of the AMBRA1/PP2A interaction, a recently published structure of the PP2A holoenzyme suggests that the structural arrangement of the PP2A-C/B subunit interface and the conformational flexibility of the PR65 subunit make the PP2A complex susceptible to structural changes that may affect substrate hydrolysis by PP2A-C or alter the substrate specificity[42–44]. It is possible that AMBRA1 binding, mediated by a PP2A consensus site, identified in this work, results in allosteric regulation of the PP2A complex structure that could mediate enhancement of the recruitment of the substrate c-Myc and increase PP2A activity on c-Myc.
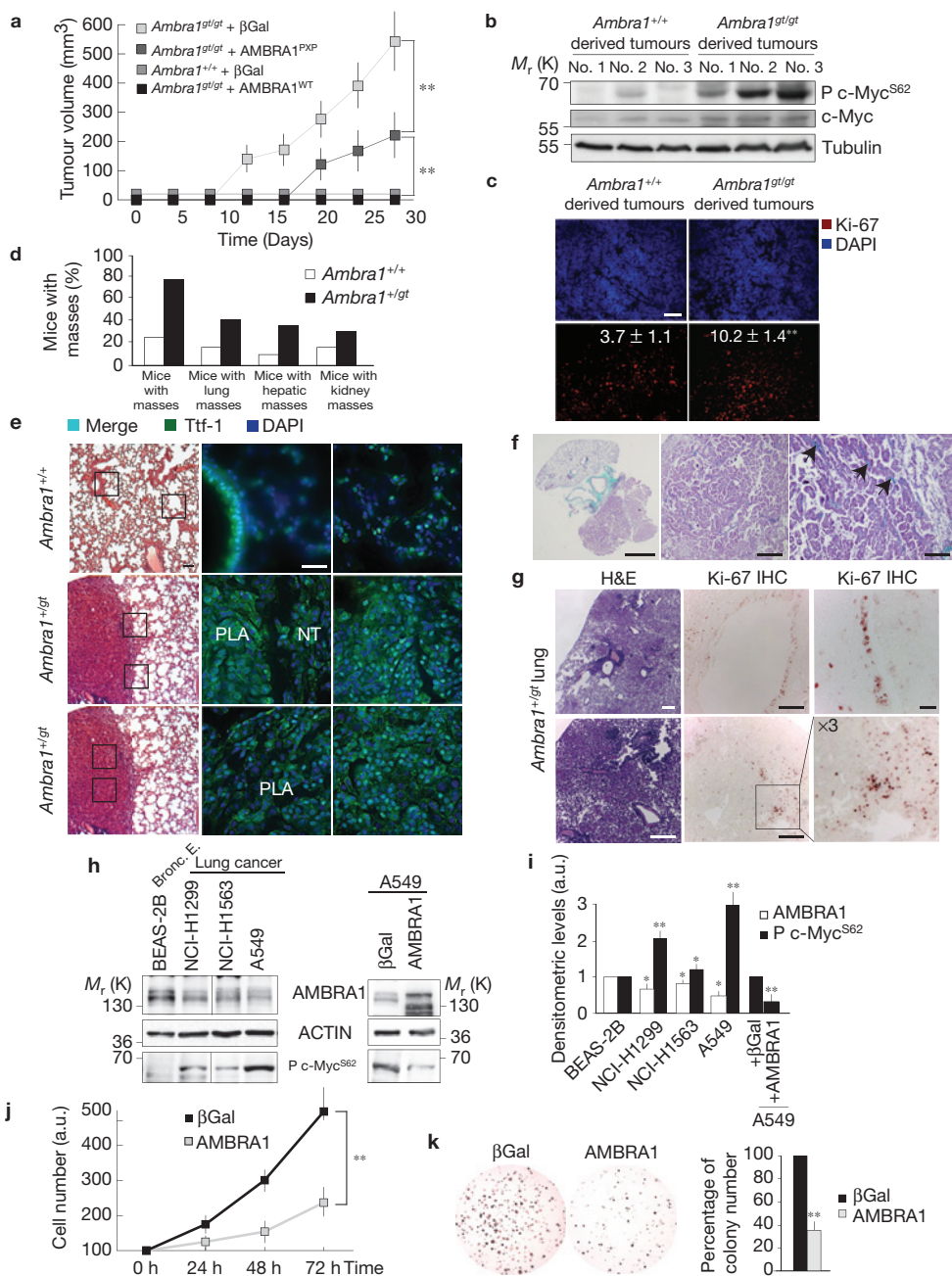
Figure 6 Ambra1 affects tumorigenesis. (**a**) MEFs *Ambra1*^{+/+} and *Ambra1*[gt/gt] were immortalized through RasV12/E1A oncogene infection. Subsequently, cells were subcutaneously injected into athymic mice and the insurgence and the size of masses were analysed. Data are presented as means ± s.d. and significance is **$P < 0.005$ ($n = 3$ independent experiments). (**b**) Protein extracts were obtained from +/+- and gt/gt-derived tumours (in **a**). The extracts were analysed by western blot, with anti-P c-Myc[S62], total c-Myc and Tubulin. (**c**) Ki-67 staining on tumours derived from +/+ and gt/gt MEFs (shown in **a**). Scale bar, 50 μm. (**d**) Analysis of the frequency of spontaneous tumours in *Ambra1*[+/gt] mice between 12 and 17 months of age. (**e**) Haematoxylin and eosin and TTF-1 (scale bars, 100 μm and 50 μm, respectively) immunofluorescence of close sections from the same mouse lung (*Ambra1*^{+/+} or *Ambra1*[+/gt]) are shown. PLA: papillary lung adenocarcinoma; NT: normal tissue. (**f**) Trichromic staining on *Ambra1*[+/gt] lung tumours. Arrowheads indicate collagen. Scale bars, 2 mm, 50 μm, 100 μm. (**g**) Ki-67 staining on lung of *Ambra1*[+/gt] mice. Haematoxylin and eosin (H&E) and immunohistochemistry (IHC), second row: tumour tissue (scale bars, 100 μm and 50 μm). IHC, first row: healthy tissue (scale bars, 50 μm and 5 μm). (**h**) Western blot analysis of AMBRA1 and P c-Myc[S62] in human adenocarcinoma cell lines. In the right panel, A549 cells were reconstituted for AMBRA1. The levels of P c-Myc[S62] were analysed by western blot. Bronc. E.: bronchiolar epithelium. The vertical line represents a splice mark of samples from the same gel. (**i**) Graph showing the correlation between AMBRA1 and P c-Myc[S62] protein levels in lung cell lines. The densitometric analysis of the western blots reported in **h** is reported in the graph. Data are presented as means ± s.d. and significance is *$P < 0.05$; **$P < 0.005$ ($n = 4$ independent experiments). (**j**) A549 cells, overexpressing AMBRA1 or βGal as a control, by retroviral infection, were analysed by MTS assay at different time points. Data are presented as means ± s.d. and significance is **$P < 0.005$ ($n = 3$ independent experiments). (**k**) The tumorigenicity of the cells used in **j** was assessed by a colony-formation assay in soft agar. Data are presented as means ± s.d. and significance is **$P < 0.005$ ($n = 4$ independent experiments). Uncropped images of blots are shown in Supplementary Fig. 7.

Also, we recently characterized AMBRA1 as a target of mTOR in the autophagy process[8]; we now show here that the AMBRA1/PP2A-mediated regulation of c-Myc is also under mTOR control. This is of the highest importance, given the key role of mTOR in regulating a cell's fate by interfering with its metabolic choices. It remains to be unveiled how mTOR exerts this control on AMBRA1, and whether this is due to direct or indirect mechanisms.

On the basis of this network regulation of cell proliferation, we also demonstrate that heterozygous disruption of the *Ambra1* locus is sufficient to induce c-Myc hyperphosphorylation and hyperproliferation, thus suggesting a correlation with tumour insurgence. In fact, AMBRA1 mutations are reported in human tumour samples and increased tumorigenesis affects *Ambra1*-mutated mice. Indeed, a well-established link between autophagy and tumorigenesis does exist[35]. The role of the autophagy core machinery components (ATG7, ATG4C) has been, indeed, dissected in tumorigenesis and in tumour progression[36–39]. In particular, a double role for autophagy has emerged in two different steps: tumour formation and maintenance. First, autophagy represents a preventive mechanism against the accumulation of damaged organelles and genome, so countering tumour formation[35–38]. Second, autophagy supplies fuel essential for established tumour growth[45–47]. Considering the place of AMBRA1 in the cascade of events leading to autophagy regulation[8,20,21], we propose that AMBRA1 plays a key role in this context, finely regulating both molecules involved in cell proliferation and in autophagy initiation. Interestingly, the tumour suppressor function of BECLIN 1 (ref. 48,49), another autophagy upstream signaller and AMBRA1 interactor[1,20], has also been associated with alternative mitogenic signalling pathways and cytokinesis that, if de-regulated, also contribute to cancer development[50].

In sum, considering the roles of the upstream autophagy signallers in tumorigenesis, we believe that great care should be taken when choosing the appropriate molecular target for clinical anticancer trials focused on autophagy inhibition[51].

Furthermore, a large body of evidence has demonstrated that c-Myc is relevant in different physiological contexts other than cancer, such as stem cell renewal and cellular differentiation[52]. Identification of the physiological role of AMBRA1 and its potential involvement in all of the above-mentioned processes will pose an interesting challenge. □

METHODS

Methods and any associated references are available in the online version of the paper.

Note: Supplementary Information is available in the online version of the paper

Published online at www.nature.com/doifinder/10.1038/ncb3072
Reprints and permissions information is available online at www.nature.com/reprints

1. Parzych, K. R. & Klionsky, D. J. An overview of autophagy: morphology, mechanism, and regulation. *Antioxid. Redox Signal.* **20,** 460–473 (2014).
2. Neufeld, T. P. Autophagy and cell growth–the yin and yang of nutrient responses. *J. Cell Sci.* **125,** 2359–2368 (2012).
3. Laplante, M. & Sabatini, D. M. mTOR signaling in growth control and disease. *Cell* **149,** 274–293 (2012).
4. Hosokawa, N. *et al.* Nutrient-dependent mTORC1 association with the ULK1-Atg13-FIP200 complex required for autophagy. *Mol. Biol. Cell* **20,** 1981–1991 (2009).
5. Jung, C. H. *et al.* ULK-Atg13-FIP200 complexes mediate mTOR signaling to the autophagy machinery. *Mol. Biol. Cell* **20,** 1992–2003 (2009).
6. Hara, T. *et al.* FIP200, a ULK-interacting protein, is required for autophagosome formation in mammalian cells. *J. Cell Biol.* **181,** 497–510 (2008).
7. Hosokawa, N. *et al.* Atg101, a novel mammalian autophagy protein interacting with Atg13. *Autophagy* **5,** 973–979 (2009).
8. Nazio, F. *et al.* mTOR inhibits autophagy by controlling ULK1 ubiquitylation, self-association and function through AMBRA1 and TRAF6. *Nat. Cell Biol.* **15,** 406–416 (2013).
9. Banreti, A., Lukacsovich, T., Csikos, G., Erdelyi, M. & Sass, M. PP2A regulates autophagy in two alternative ways in *Drosophila. Autophagy* **8,** 623–636 (2012).
10. Sutter, B. M., Wu, X., Laxman, S. & Tu, B. P. Methionine inhibits autophagy and promotes growth by inducing the SAM-responsive methylation of PP2A. *Cell* **154,** 403–415 (2013).
11. Puustinen, P. *et al.* CIP2A oncoprotein controls cell growth and autophagy through mTORC1 activation. *J. Cell Biol.* **204,** 713–727 (2014).
12. Eichhorn, P. J., Creyghton, M. P. & Bernards, R. Protein phosphatase 2A regulatory subunits and cancer. *Biochim. Biophys. Acta* **1795,** 1–15 (2009).
13. Virshup, D. M. & Shenolikar, S. From promiscuity to precision: protein phosphatases get a makeover. *Mol. Cell* **33,** 537–545 (2009).
14. Arroyo, J. D. & Hahn, W. C. Involvement of PP2A in viral and cellular transformation. *Oncogene* **24,** 7746–7755 (2005).
15. Janssens, V. & Goris, J. Protein phosphatase 2A: a highly regulated family of serine/threonine phosphatases implicated in cell growth and signalling. *Biochem. J.* **353,** 417–439 (2001).
16. Janssens, V., Goris, J. & Van Hoof, C. PP2A: the expected tumor suppressor. *Curr. Opin. Genet. Dev.* **15,** 34–41 (2005).
17. Sears, R. *et al.* Multiple Ras-dependent phosphorylation pathways regulate Myc protein stability. *Genes Dev.* **14,** 2501–2514 (2000).
18. Yeh, E. *et al.* A signalling pathway controlling c-Myc degradation that impacts oncogenic transformation of human cells. *Nat. Cell Biol.* **6,** 308–318 (2004).
19. Junttila, M. R. & Westermarck, J. Mechanisms of MYC stabilization in human malignancies. *Cell Cycle* **7,** 592–596 (2008).
20. Fimia, G. M. *et al.* Ambra1 regulates autophagy and development of the nervous system. *Nature* **447,** 1121–1125 (2007).
21. Di Bartolomeo, S. *et al.* The dynamic interaction of AMBRA1 with the dynein motor complex regulates mammalian autophagy. *J. Cell Biol.* **191,** 155–168 (2010).
22. Cecconi, F. & Levine, B. The role of autophagy in mammalian development: cell makeover rather than cell death. *Dev. Cell* **15,** 344–357 (2008).
23. Benato, F. *et al.* Ambra1 knockdown in zebrafish leads to incomplete development due to severe defects in organogenesis. *Autophagy* **9,** 476–495 (2013).
24. Malumbres, M. & Barbacid, M. Cell cycle, CDKs and cancer: a changing paradigm. *Nat. Rev. Cancer* **9,** 153–166 (2009).
25. Hara, K. *et al.* Raptor, a binding partner of target of rapamycin (TOR), mediates TOR action. *Cell* **110,** 177–189 (2002).
26. Jayadeva, G. *et al.* B55alpha PP2A holoenzymes modulate the phosphorylation status of the retinoblastoma-related protein p107 and its activation. *J. Biol. Chem.* **285,** 29863–29873 (2010).

27. Zhang, H. *et al.* Loss of Tsc1/Tsc2 activates mTOR and disrupts PI3K-Akt signaling through downregulation of PDGFR. *J. Clin. Invest.* **112,** 1223–1233 (2003).
28. Dyson, H. J. & Wright, P. E. Intrinsically unstructured proteins and their functions. *Nat. Rev. Mol. Cell Biol.* **6,** 197–208 (2005).
29. Lim, W. A., Richards, F. M. & Fox, R. O. Structural determinants of peptide-binding orientation and of sequence specificity in SH3 domains. *Nature* **372,** 375–379 (1994).
30. Evans, B. J. *et al.* Physical association of GPR54 C-terminal with protein phosphatase 2A. *Biochem. Biophys. Res. Commun.* **377,** 1067–1071 (2008).
31. Holzinger, A. *et al.* Monoclonal antibody to thyroid transcription factor-1: production, characterization, and usefulness in tumor diagnosis. *Hybridoma* **15,** 49–53 (1996).
32. Szabo, E. Lung epithelial proliferation: a biomarker for chemoprevention trials? *J. Natl Cancer Inst.* **93,** 1042–1043 (2001).
33. Kauffman, S. L. Cell proliferation in the mammalian lung. *Int. Rev. Exp. Pathol.* **22,** 131–191 (1980).
34. Ayers, M. M. & Jeffery, P. K. Proliferation and differentiation in mammalian airway epithelium. *Eur. Respir. J.* **1,** 58–80 (1988).
35. White, E. Deconvoluting the context-dependent role for autophagy in cancer. *Nat. Rev. Cancer* **12,** 401–410 (2012).
36. Mathew, R. *et al.* Autophagy suppresses tumorigenesis through elimination of p62. *Cell* **137,** 1062–1075 (2009).
37. Marino, G. *et al.* Tissue-specific autophagy alterations and increased tumorigenesis in mice deficient in Atg4C/autophagin-3. *J. Biol. Chem.* **282,** 18573–18583 (2007).
38. Takamura, A. *et al.* Autophagy-deficient mice develop multiple liver tumors. *Genes Dev.* **25,** 795–800 (2011).
39. Inami, Y. *et al.* Persistent activation of Nrf2 through p62 in hepatocellular carcinoma cells. *J. Cell Biol.* **193,** 275–284 (2011).
40. Sontag, E. Protein phosphatase 2A: the Trojan Horse of cellular signaling. *Cell Signal.* **13,** 7–16 (2001).
41. Kolupaeva, V. & Janssens, V. PP1 and PP2A phosphatases–cooperating partners in modulating retinoblastoma protein activation. *FEBS J.* **280,** 627–643 (2013).
42. Millward, T. A., Zolnierowicz, S. & Hemmings, B. A. Regulation of protein kinase cascades by protein phosphatase 2A. *Trends Biochem. Sci.* **24,** 186–191 (1999).
43. Cho, U. S. & Xu, W. Crystal structure of a protein phosphatase 2A heterotrimeric holoenzyme. *Nature* **445,** 53–57 (2007).
44. Xu, Y. *et al.* Structure of the protein phosphatase 2A holoenzyme. *Cell* **127,** 1239–1251 (2006).
45. Mathew, R. & White, E. Autophagy in tumorigenesis and energy metabolism: friend by day, foe by night. *Curr. Opin. Genet. Dev.* **21,** 113–119 (2011).
46. Guo, J. Y. *et al.* Autophagy suppresses progression of K-ras-induced lung tumors to oncocytomas and maintains lipid homeostasis. *Genes Dev.* **27,** 1447–1461 (2013).
47. Guo, J. Y. *et al.* Activated Ras requires autophagy to maintain oxidative metabolism and tumorigenesis. *Genes Dev.* **25,** 460–470 (2011).
48. Qu, X. *et al.* Promotion of tumorigenesis by heterozygous disruption of the beclin 1 autophagy gene. *J. Clin. Invest* **112,** 1809–1820 (2003).
49. Liang, X. H. *et al.* Induction of autophagy and inhibition of tumorigenesis by beclin 1. *Nature* **402,** 672–676 (1999).
50. Thoresen, S. B., Pedersen, N. M., Liestol, K. & Stenmark, H. A phosphatidylinositol 3-kinase class III sub-complex containing VPS15, VPS34, Beclin 1, UVRAG and BIF-1 regulates cytokinesis and degradative endocytic traffic. *Exp. Cell Res.* **316,** 3368–3378 (2010).
51. Helgason, G. V., Holyoake, T. L. & Ryan, K. M. Role of autophagy in cancer prevention, development and therapy. *Essays Biochem.* **55,** 133–151 (2013).
52. Smith, K. & Dalton, S. Myc transcription factors: key regulators behind establishment and maintenance of pluripotency. *Regen. Med.* **5,** 947–959 (2010).
53. Burgess, A. *et al.* Loss of human Greatwall results in G2 arrest and multiple mitotic defects due to deregulation of the cyclin B-Cdc2/PP2A balance. *Proc. Natl Acad. Sci. USA* **107,** 12564–12569 (2010).

METHODS

Cell culture and reagents. HEK293, MEFs and HeLa cells were cultured in Dulbecco's modified Eagle's medium (DMEM, Sigma Aldrich) supplemented with 10% fetal bovine serum (FBS, GIBCO), 2 mM L-glutamine, 1% penicillin/streptomycin solution at 37 °C. Human lung and breast carcinoma cell lines, with respective control cells, were purchased from the American Type Culture Collection (ATCC) and cultured according to the supplier's instructions. For autophagy induction and for amino-acid starvation, cells were washed with PBS and cultured for 1–3 h in Earle's balanced salt solution (EBSS; Sigma-Aldrich) or in medium without amino acids (GIBCO), respectively. When indicated, cells were incubated in the presence of 50 µg ml^{-1} cycloheximide (CHX, Sigma-Aldrich), 2 µM rapamycin (Sigma Aldrich), 1.5 µM Torin1 (Tocris). HeLa and HEK293 cells were transiently transfected with expression vectors using Lipofectamine 2000 (Invitrogen) as indicated by the supplier. Viral infection of A549 and MCF-7 cells with the retroviral AMBRA1-coding construct was performed as previously described[8].

Plasmid constructs. Constructs coding for AMBRA1 and its deletion mutants (Flag–AMBRA1ΔWD40, Myc–F1, Myc–F2, Myc–F3, Myc–F1ΔWD40, Myc–F3a, Myc–F3b) or AMBRA1 site-specific mutants (AMBRA1^{NT-PXP}, AMBRA1^{CT-PXP}, AMBRA1^{PXP}) were cloned in pLPCX vector[8,19,20] (Clontech). Plasmid encoding Flag–PR65A was provided by A. C. Gingras. c-Myc construct was cloned in pLPCX vector by using V5–Flag–c-Myc as a template (provided by R. Sears). c-Myc encoding sequence was amplified by PCR and cloned in the acceptor vector by using EcoRI and NotI restriction sites. c-Myc^{S62D} mutant and AMBRA1^{PXP} mutants were created by site-directed mutagenesis (Agilent), using c-Myc and AMBRA1 as templates, respectively.

Antibodies. All of the antibodies were used at a dilution of 1:1,000 unless specified otherwise. Anti-Flag (cat. no. F3165; 1:2,000), β tubulin (cat. no. T4026; 1:3,000) and anti-ACTIN (cat. no. A2066; 1:2,000) were from Sigma Aldrich. Anti-c-Myc (9E10, cat. no. sc-40), anti-c-Myc (N272, cat. no. sc-764), anti c-Myc (C33, cat. no. sc-42), anti-ULK1 (cat. no. sc-33182), anti-BECLIN 1 (cat. no. sc-10086 and sc-11427), anti-PR65A (cat. no. sc-15355), anti-P AKT (cat. no. sc-16646), anti-AKT (cat. no. sc-8312), anti-GSK3β (cat. no. 377213), anti-P GSK3β (cat. no. sc-11757), anti-ERK1/2 (cat. no. 292838), anti-P ERK1/2 (cat. no. sc-16982), anti-Cyclin D (cat. no. sc-182), anti-Cyclin E (cat. no. sc-20684), anti-Cyclin B (cat. no. sc-245), anti-Cyclin A (cat. no. sc-596), anti-P62 (cat. no. sc-28359; 1:3,000) and anti-HSP 90 (cat. no. sc-7947; 1:3,000) were from Santa Cruz. Anti-AMBRA1 (cat. no. 26190002; 1:3,000) used on human extracts was from Novus. Anti-Ambra1 (used on mouse extracts, cat. no. ABC131) and anti-PP2A-C (1D6, cat. no. 05-421) were from MERCK Millipore. Anti-P c-Myc^{S62} (cat. no. ab78318; 1:500) was from Abcam. Anti-P RPS6 (cat. no. 5364; 1:3,000), anti-LC3 (cat. no. 3868; 1:6,000) and anti-RAPTOR (cat. no. 2280) were from Cell Signaling. For immunohistochemistry analysis, anti-P62 (ct. no. PM045; 1:2,000) from MBL was used. Anti-Ki-67 (SP6, cat no. RM-9106; 1:2,000) was from Thermo Scientific. Anti-TTF-1 (cat no. 8G7GG3/1; 1:100) was from Dako.

RNA interference. RNA interference was performed using the AMBRA1 and control siRNA oligonucleotides that were previously described[8,20]. RAPTOR (cat. no. M-004107-01) and c-Myc (cat. no. AM16704) siRNAs were purchased from Dharmacon and LifeTechnologies, respectively. Cells (2×10^5 per well) were transfected with 100 pmol siRNA in 6-well plates by Lipofectamine 2000 (Invitrogen), as suggested by the supplier. Where indicated, 24 h after the AMBRA1-siRNA treatment, AMBRA1 constructs (AMBRA1^{WT} or AMBRA1^{PXP}) or βGal or c-Myc constructs (c-Myc^{WT} or c-Myc^{S62D}) were transiently expressed. Where indicated, 24 h after the AMBRA1-siRNA treatment, RAPTOR- or CTRL-siRNA were transfected in depleted cells.

Immunoblotting. Cell lysates were prepared with RIPA buffer. Mouse tissues were homogenized mechanically in tissue lysis buffer (50 mM Tris HCl pH 7.5, 320 mM sucrose, 50 mM NaCl, 1% Triton X-100 and protease and phosphatase inhibitors). Homogenates were centrifuged at 12,000g at 4 °C for 30 min and supernatants were collected. Protein extracts were quantified by Lowry protein assay (Biorad), and denatured by adding Laemmli buffer (0.1% bromophenol blue, 10% glycerol, 2% SDS, 5% ß-mercaptoethanol, 270 mM Tris HCl pH 6.8). A total of 30–50 µg of proteins was analysed by SDS–polyacrylamide gel electrophoresis and immunoblotting. Proteins were separated on acrylamide gel (Biorad) and electroblotted onto nitrocellulose membranes (Protran, Schleicher & Schuell). Blots were incubated with primary antibodies in 5% non-fat dry milk in PBS plus 0.1% Tween-20 overnight at 4 °C. Detection was achieved using horseradish-peroxidase-conjugate secondary antibody (Biorad) and visualized with ECL plus (Amersham Bioscience). For the western blot analysis of immunoprecipitated c-Myc, TrueBlot secondary antibody (EBioscience) was used, to minimize detection of immunoglobulins in the immunoprecipitation samples.

Immunoprecipitation. Cells were lysed in CHAPS buffer (40 mM Hepes pH 7.4, 150 mM NaCl, 2 mM EDTA, 10 mM β-glycerophosphate, 0.3% CHAPS and protease and phosphatase inhibitors). Lysates (1–3 mg) were then incubated at 4 °C for 30 min, and following centrifugation at 4 °C for 15 min at 12,000g to remove insoluble debris, and equal amounts of proteins were incubated with 1–2 µg of monoclonal anti-c-Myc or anti PP2A-C antibodies for at least 2–3 h. In the case of Flag–PR65A immunoprecipitation, anti-Flag-conjugated agarose beads were used (Sigma Aldrich). Then, protein-G-conjugated Sepharose beads (Roche) were added to anti-c-Myc (C-33) and anti-PP2A-C primary antibodies, and incubated with rotation at 4 °C for 1 h. The beads were finally collected by centrifugation and washed four times with the lysis buffer plus 150 mM NaCl. Proteins bound to the beads were eluted with 20 µl of SDS–PAGE sample buffer and boiled at 95 °C for 10 min.

Phosphatase assay. For phosphatase assay, P c-Myc^{S62}-enriched[54] HeLa cells were suspended in lysis buffer (50 mM Tris-HCl, pH 7.4, 7.5% glycerol, 1 mM EDTA, 150 mM NaCl, 0.5% Nonidet P-40, 1 mM Na$_3$VO$_4$, Complete protease inhibitor), incubated for 30 min in ice and cleared from debris by centrifugation and incubated with c-Myc antibody (C-33, mouse monoclonal, Santa Cruz) followed by incubation with G protein Sepharose beads (Roche). The obtained immunocomplex was washed in lysis buffer without Na$_3$VO$_4$. Wild-type or *Ambra1$^{gt/gt}$* MEFs were lysed in NET buffer (50 mM Tris-HCl, pH 7.4, 150 mM NaCl, 1% Nonidet P-40, 15 mM EDTA, Complete Protease Inhibitor). The catalytic subunit of the PP2A phosphatase (PP2A-C) was immunoprecipitated from wild-type or *Ambra1$^{gt/gt}$* protein extracts by using anti PP2A-C antibody (1D6, mouse monoclonal, Millipore). The same amount of c-Myc was added to PP2A-C coming from wild-type or *Ambra1$^{gt/gt}$* cells and the phosphatase reaction was carried out *in vitro*, for 15 min at 37 °C, in the 'phosphatase reaction' buffer (50 mM Tris-HCl, pH 7.4, and 2 mM dithiothreitol). As a negative control, c-Myc was incubated with an immunoprecipitation carried out with mouse immunoglobulin mix (SIGMA), and treated as PP2A-C immunocomplexes. The products of the phosphatase reactions were boiled for 10 min at 95 °C in Laemmli buffer and subsequently analysed by western blot, by using antibodies against P c-Myc^{S62}, total c-Myc and PP2A-C. A similar PP2A phosphatase assay protocol was already reported[52]. TrueBlot secondary antibody (EBioscience) was used to minimize the detection of the immunoglobulins in the immunoprecipitation samples.

Size-exclusion chromatography. Four milligrams of HeLa endogenous extract was injected onto a Superose 6 HR 10/30 fast protein liquid chromatography (FPLC) gel filtration column (GE Healthcare), equilibrated with 20 mM Tris-HCl (pH 7.5), 200 mM NaCl, 12.5% glycerol, 0.2% Nonidet P-40, 1 mM EDTA, 1 mM EGTA and 1 mM dithiothreitol, and eluted at a flow rate of 0.25 ml min^{-1} with the same buffer. Proteins were collected in 250 µl fractions, precipitated with 10% trichloroacetic acid (TCA), and subjected to western blotting. Gel filtration columns were calibrated with the following molecular mass markers: thyroglobulin (relative molecular mass 669,000 (M_r 669K)), apoferritin (M_r 443K), β-amylase (M_r 200K), alcohol dehydrogenase (M_r 150K), bovine serum albumin (M_r 66K), and carbonic anhydrase (M_r 29K) (Sigma Aldrich).

Immunocytochemistry. Cells were washed in PBS and fixed with 4% paraformaldehyde in PBS for 15 min. After permeabilization with 0.2% Triton X-100 in PBS for 5 min, cells were blocked in 2% horse serum in PBS and incubated for 1–2 h at room temperature, with the primary antibodies. We used antibody directed against the P c-Myc^{S62} or against BrdU. Cells were then washed and incubated for 1 h with labelled anti-mouse (Alexa Fluor-488 or −555, Molecular Probes) secondary antibodies. Images were examined under a Leica TCS SP5 confocal microscope equipped with a ×63 oil-immersion objective.

Immunohistochemistry for Ki-67 and for p62 was carried out on lung and liver paraffin sections using a monoclonal anti-Ki-67 from rabbit (Clone SP6, Thermo Scientific) and a polyclonal rabbit-anti-p62 affinity purified (MBL). Antigen retrieval was performed using citrate buffer incubation in the microwave for both antigens. Antibody incubation was carried out overnight at 4 °C (Ki-67) or 1:1,000 (p62) and immunoreactions were finally developed and visualized using the avidin–biotin–AEC method (Ki-67) or the Envision-DAB method (p62). In the case of the xenografts and TTF-1 staining on lung, tissue samples were fixed in 4% paraformaldehyde (PFA) and embedded in Tissue-Tek OCT compound (Sakura Finetechnical). Sections were prepared and incubated with Ki-67 and TTF-1 primary antibodies overnight at 4 °C. The day after, labelled Alexa Fluor-488 (Molecular Probes, Eugene, OR) secondary antibody was used. Where indicated, haematoxylin and eosin and trichromic staining procedures were carried out, according to standard protocols.

MTS assay. For the MTS assay (Promega), HeLa cells were knocked down and transfected as previously described. Following 6 h Lipofectamine transfection, cells were split and 5,000 cells were plated in each well of a 96-well plate. Transformed MEFs were plated in a 96-well plate at a cellular density of 7,000 cells per well. Each sample was analysed in triplicate. MTS assay was performed as indicated by the supplier.

BrdU incorporation assay. Cells were pulsed with BrdU for 1 h at a final concentration of 100 µM. Following incubation with BrdU, cells were fixed in cold methanol for 20 min at −20 °C and then rehydrated in phosphate saline buffer (PBS). HCl (2 M) was added to each well and incubated at room temperature for 30 min. Cells were washed twice for 5 min in 0.1 M sodium borate (pH 8.5) and washed for 5 min in PBS before blocking in 2% bovine serum albumin (BSA/PBS) for 1 h at room temperature. Anti-BrdU was diluted at 1:100 in 2% BSA/PBS and added to each well and incubated at 4 °C overnight. Coverslips were washed three times in PBS for 5 min and antibody–antigen complexes were detected with Alexa Fluor 488-conjugated goat anti-mouse antibody diluted 1:500 in 2% BSA/PBS and incubated at room temperature for 1 h. Cells were then washed four times with PBS and counterstained with 4′,6-diamidino-2-phenylindol (DAPI) for 5 min at room temperature in the dark. Finally, cells were mounted in GEL/MOUNT antifade (Biomeda), and visualized with an Olympus IX70 microscope using softWoRx and a Delta Vision Imaging Workstation. The *in vitro* experiments were performed on 3–4 clones for each MEF genotype.

Mice. *Ambra1* heterozygous (*Ambra1$^{+/gt}$*) mice[20] and wild-type littermates were used for the analysis of spontaneous tumorigenesis. Both female and male mice from CD1 and mixed (C57BL/6 × CD1) strains were used. Necropsies were performed on 40 *Ambra1$^{gt/+}$* and 40 wild-type mice, aged 12–17 months and the masses that were present on gross examination were recorded. Experiments were carried out in accordance with the European Community's Council Directive 86/609/EEC. Formal approval of these experiments was obtained from the Italian Ministry of Health (D.L.vo 116/92).

Identification of *AMBRA1* genomic alteration in human tumours. Mutations and chromosome alterations in the TCGA data set of human tumours from the endometrium (sample size: 227), the large intestine (sample size: 723) and the urinary tract (sample size: 102) are available at cancergenome.nih.gov.

Zebrafish. Zebrafish handling and treatment were approved by the UniPD Ethical Committee on Animal Experimentation (CEASA – Project no. 25/2012). Cell transplantation experiments were performed as described previously[55]. In brief, embryos were injected, at the one-cell stage, with a mixture containing 200 pg EGFP mRNA (for *in vivo* tracking of trans-planted cells) and 10 ng biotin–dextran lysine fixable (10.000 Mw, Sigma) alone (control donors) or in combination with designated MOs: 10 ng MO1-ambra1a; 20 ng MO1-ambra1b; 2.5 ng MO1-ambra1a + 5 ng MO1-ambra1b mixture.

At blastula stage (4 hpf), donor and wild-type host embryos were manually dechorionated. Approximately 30 cells from donor embryos were then transplanted into host embryos. Transplanted embryos were fixed in paraformaldehyde 4% in phosphate buffered saline, for 2 h at room temperature, at 90% epiboly (9 hpf). Biotin-injected transplanted cells were detected in hosts using an avidin–biotinylated complex (ABC Kit, Vectastain) and the DAB substrate. Proliferation was analysed by whole-mount immunohistochemistry with anti-phosphohistone H3 antibody (polyclonal rabbit Millipore) according to the manufacturer's instructions and revealed with NBT/BCIP solution (Roche).

For imaging a confocal microscope (Leica SP5) was used. Quantitative data are expressed as mean ± s.e.m. Statistical significance was determined by χ-squared test using the Primer statistical software.

Real-time PCR. RNA was isolated by using the RNeasy Micro Kit (Qiagen), according to the manufacturer's instructions. Real-time PCR was performed by using the SensiMix Plus SYBR Kit (Quantace). The primer sets used were as follows: mouse Cyclin A forward, 5′-TGCAAACTGTAAGGTTGAAAGC-3′, and reverse, 5′-TGTAGAGAGCCAAGTGGAAGG-3′; mouse Cyclin B forward, 5′-CTGCAGTG ACTACGTGAAGG-3′, and reverse 5′-TGTGGATTAATGGACTGTAAAACC-3′; mouse Ambra1 forward, 5′-CTACTGGGACCAGCTAAGTGAAA-3′, and reverse 5′-ACGTGGCTCTGCTGGTTC-3′. Real-time quantification was performed by using a Fast-Real Time PCR System (Applied Biosystems). Data were normalized to β-actin. Fold-change was determined by using the 2-ΔΔCT method and all reactions were performed in triplicate.

Tumour xenografts. Wild-type or *Ambra1$^{gt/gt}$* MEFs were transformed by pBABE encoding RasV12/E1A oncogenes. Tumours were induced by subcutaneous injection in nude mice of 5×10^6 cells. Transformed MEFs wild-type, *Ambra1$^{gt/gt}$*, *Ambra1$^{gt/gt}$* infected with *AMBRA1^{WT}* or *AMBRA1^{PXP}* retroviral constructs were suspended in PBS supplemented with 0.1% glucose. βGal retroviral construct was used as a control in wild-type, Ambra1$^{gt/gt}$ MEFs. Tumours were measured with external calipers, and the volume was calculated as $(4\pi/3) \times (\text{width}/2)^2 \times (\text{length}/2)$. Twenty-eight days after injection of the cells, animals were killed and all tumours were excised. Samples from tumours xenografts were dissected and frozen for further analysis.

Colony formation in soft-agar assay. The colony-formation assay in soft agar was performed by using the CytoSelect 96-Well Cell Transformation Assay, as indicated by the supplier. For AMBRA1-overexpressing A549 and MCF-7 cells, 0.5×10^4 cells were seeded in 12-well plates. The colony growth was monitored day by day and colonies were counted 18 and 12 days after, respectively. Representative images were acquired using bright-field microscopy.

Yeast two-hybrid assay. The results of the yeast two-hybrid assay shown in Fig. 2 come from the same data set reported in our previous publication: refer to this reference for the methods[20].

Tandem affinity purification assay. The results of the tandem affinity purification shown in Supplementary Table 1 come from the same data set reported in our previous publication: refer to this reference for the methods[8].

Statistical analysis. For all experiments shown, *n* is indicated in the figure legends. Each point value reported in the graphs represents the mean ± s.d. or ± s.e.m, as indicated in the figure legends. Statistical significance was measured by an unpaired two-tailed *t*-test. *P* < 0.05 is considered significant.

No statistical method or inclusion/exclusion criteria were used to predetermine sample size or define the experimental group. The experiments were not randomized. The investigators were not blinded to allocation during experiments and outcome assessment.

For the experiments in which no quantification is shown, images representative of at least 3 independent experiments are shown.

54. Junttila, M. R. *et al.* CIP2A inhibits PP2A in human malignancies. *Cell* **130,** 51–62 (2007).
55. Nusslein-Volhard, C. & Dahm, R. *Zebrafish. A Practical Approach* (Oxford Univ. Press, 2002).
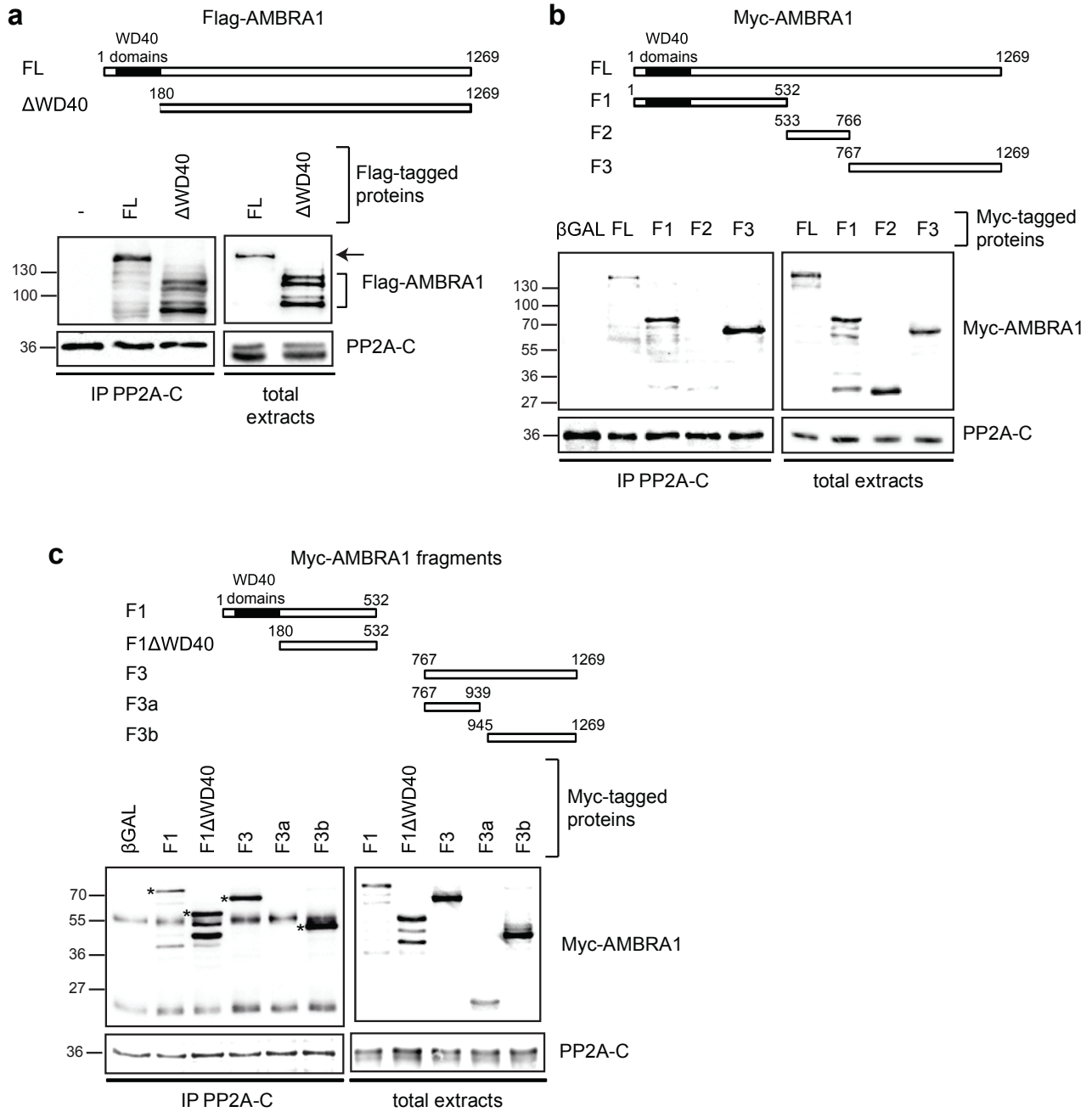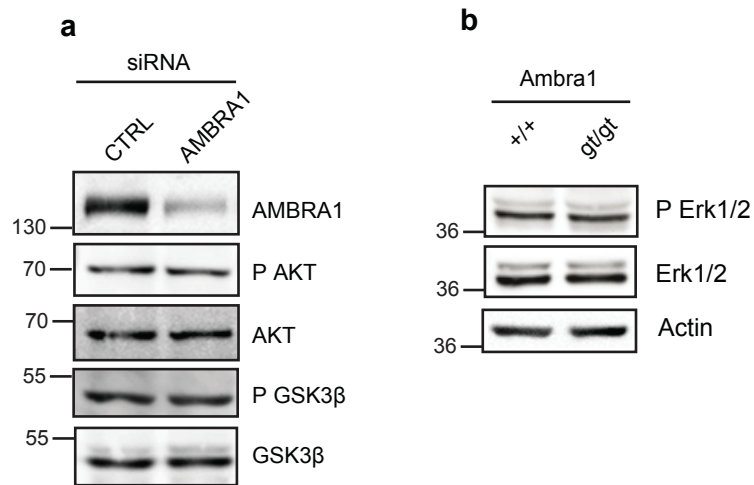
Supplementary Figure 1 Characterization of the interaction region between AMBRA1 and PP2A **a)** HEK293 cells were transfected with vectors encoding for Flag-AMBRA1 and Flag-WD40 AMBRA1. Protein extracts were immunoprecipitated using an anti-PP2A-C antibody. Purified complexes and corresponding total extracts were analysed by western blot using an anti-Flag and anti-PP2A-C antibodies. The arrow and the bracket indicate bands corresponding to Flag-AMBRA1 and Flag-WD40 AMBRA1, respectively. **b)** HEK293 cells were transfected with vectors encoding for Myc-AMBRA1 and AMBRA1 deletion constructs, called Myc-F1, Myc-F2, Myc-F3. Protein extracts were immunoprecipitated using an anti-PP2A-C antibody. Purified complexes and corresponding total extracts were analysed by western blot using an anti-Myc and anti-PP2A-C antibodies. **c)** HEK293 cells were transfected with vectors encoding for AMBRA1 deletion constructs called Myc-F1, Myc-F1ΔWD40, Myc-F3, Myc-F3a and Myc-F3b. Protein extracts were treated as in **a**. Asterisks (*) indicate the specific bands.
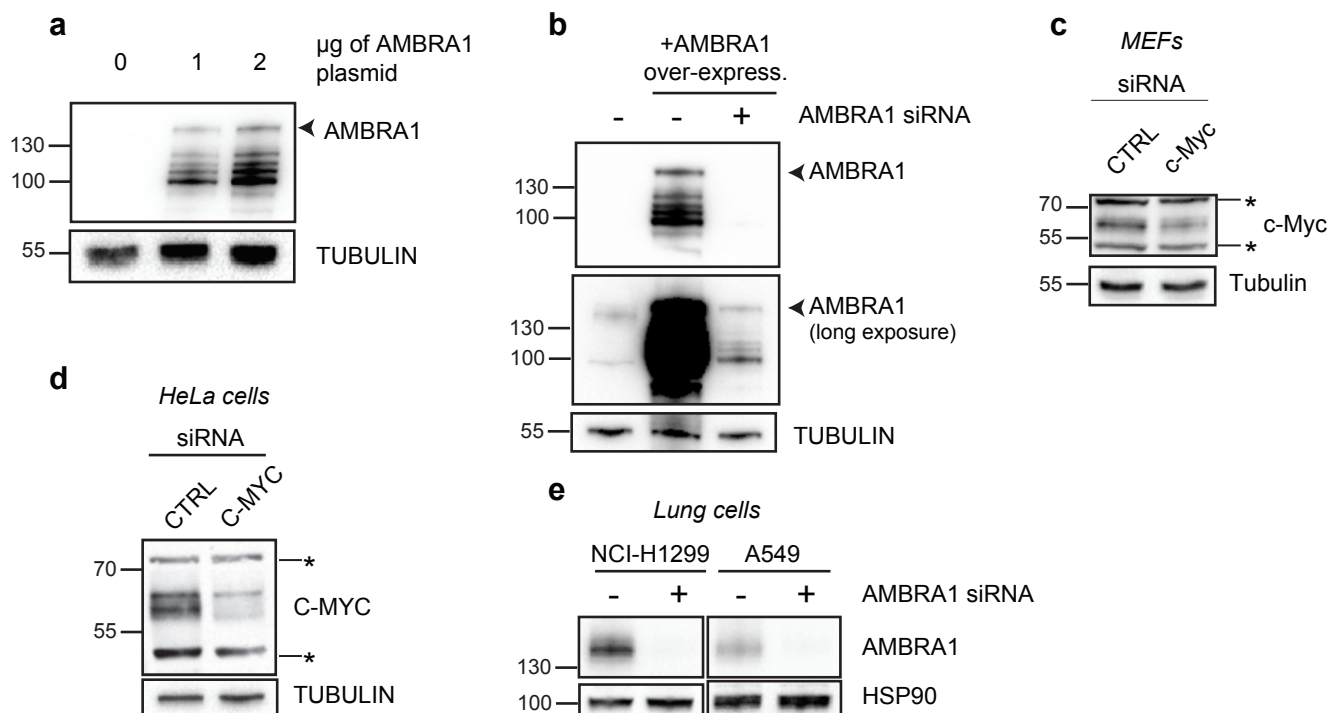
Supplementary Figure 2 Analysis of the banding patterns of overexpressed AMBRA1 and endogenous C-MYC **a)** HeLa cells were transfected with increasing concentrations of AMBRA1 cDNAs. Protein extracts were analysed by Western Blot analysis using antibodies against AMBRA1 and TUBULIN. Different bands can be appreciated upon AMBRA1 over-expression, with the band indicated by the arrowhead corresponding to the expected size-range for full-length AMBRA1. The other bands, with lower molecular weights, correspond to AMBRA1 full-length cleavage products. **b)** HeLa cells were transfected with control oligos and plasmid (first lane), AMBRA1 cDNA alone (second lane) or AMBRA1 cDNA in combination with siRNA against AMBRA1 (third lane). Protein extracts were analysed by Western Blot analysis with the same antibodies as in **b**. **c)** Primary MEFs have been knocked-down for c-Myc by specific siRNAs (c-Myc siRNA); unspecific oligos have been used as a control (CTRL siRNA). Protein extracts were analysed by Western Blot using antibodies against c-Myc (anti-c-Myc N262) and Tubulin. Unspecific bands [indicated by asterisks (*)] are not affected by c-Myc siRNA, while central bands, corresponding

to c-Myc protein, are down-regulated by the c-Myc siRNA treatment. We did not report the unspecific bands in the c-Myc Western Blots throughout the manuscript for a major clarity. **d)** HeLa cells have been knocked-down for C-MYC by specific siRNAs (C-MYC siRNA); unspecific oligos have been used as a control (CTRL siRNA). Protein extracts were analysed by Western Blot using antibodies against C-MYC (anti C-MYC N262) and Tubulin. Unspecific bands [indicated by asterisks (*)] are not affected by C-MYC siRNA, while central bands, corresponding to C-MYC protein, are down-regulated by the C-MYC siRNA treatment. We did not report the unspecific bands in the C-MYC Western Blots throughout the manuscript for a major clarity. Two exposure of the same Western Blot are shown: in the longer exposure it is possible to appreciate the residual signal corresponding to overexpressed AMBRA1 in silenced cells (third lane), probably due to a small percentage of cells not transfected with the siRNA. **e)** NCI-H1299 and A549 cells were knocked-down for AMBRA1 and protein extracts were analysed by Western Blot using antibodies against AMBRA1 and HSP90, as a loading control.

a

siRNA

CTRL   AMBRA1

130 —	AMBRA1
70 —	P AKT
70 —	AKT
55 —	P GSK3β
55 —	GSK3β

b

Ambra1

+/+   gt/gt

36 —	P Erk1/2
36 —	Erk1/2
36 —	Actin

Supplementary Figure 3 Analysis of c-Myc regulators and PP2A-C substrates in AMBRA1-defective cells **a)** Protein extracts from AMBRA1 knocked-down cells were analysed by western blot using antibodies against AKT, phospho-AKT, GSK3B and phospho-GSK3B. **b)** Western blot analysis of phospho-Erk1/2 and total Erk1/2 in *Ambra1*^{+/+} and *Ambra1*^{gt/gt} MEFs.
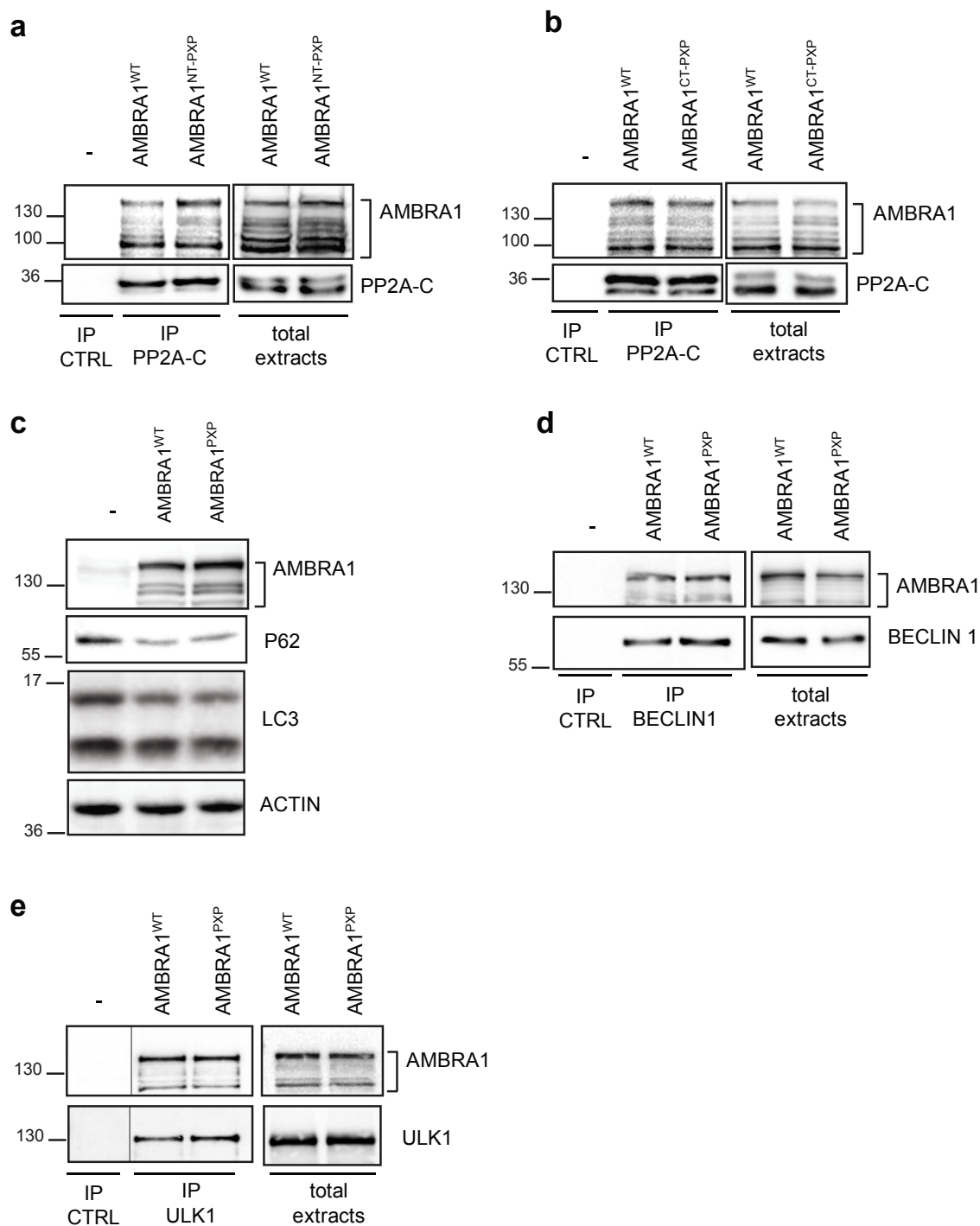
Supplementary Figure 4 Characterization of AMBRA1[NT-PX] and AMBRA1[CT-PXP] mutants **a)** HEK293 cells were transfected with vectors encoding for AMBRA1[WT] and AMBRA1[NT-PXP]. Protein extracts were immunoprecipitated using an anti-PP2A-C antibody and the immunocomplexes were analysed by western blot, using an anti-AMBRA1 and anti-PP2A-C antibodies. **b)** HEK293 cells were transfected with vectors encoding for AMBRA1[WT] and AMBRA1[CT-PXP]. Protein extracts were treated as in **a. c)** HeLa cells, transfected with βGal, as a control, AMBRA1[WT] or AMBRA1[PXP], were lysed and proteins extracts were analysed for p62 levels and LC3I to LC3II conversion by western blot analysis. **d)** HEK293 cells were transfected with vectors encoding for AMBRA1[WT] and AMBRA1[PXP]. Endogenous BECLIN 1 was immunoprecipitated from protein extracts and the immunocomplexes were analysed by western blot, using antibodies against BECLIN 1 and AMBRA1. **e)** HEK293 cells were transfected as in **d**. Endogenous ULK1 was immunoprecipitated from protein extracts and the immunocomplexes were analysed by western blot, using antibodies against ULK1 and AMBRA1. The vertical line represents a splice mark of samples on the same gel. The brackets indicate bands corresponding to over-expressed AMBRA1.
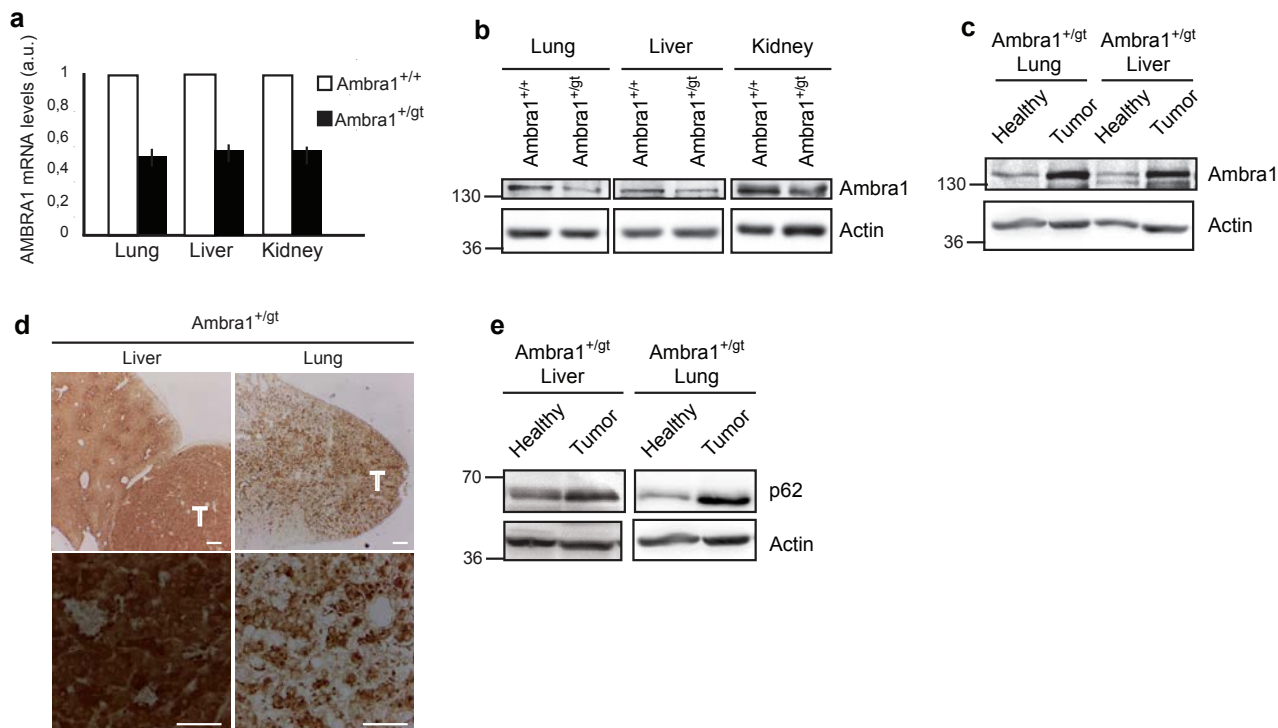
Supplementary Figure 5 Analysis of Ambra1 levels, cell proliferation and autophagy in Ambra1$^{+/gt}$ mice **a)** Analysis of Ambra1-mRNA levels in tissues of, wild-type (+/+) and heterozygous (+/gt) 3-months old *Ambra1* mice. Data are presented as means±s.e.m. and significance is **P<0.005 (n=3 mice per each genotype). **b)** We extracted proteins from lung, liver and kidney organs of wild-type or heterozygous for *Ambra1* 3-months old mice. Ambra1 levels were analysed by western blot using an anti-Ambra1 and anti-Actin antibody. **c)** Analysis of Ambra1 levels in lung and liver organs from wild-type (Ambra1$^{+/+}$) or heterozygous (Ambra1$^{+/gt}$) mice. We selected both tumour tissue and the surrounding healthy tissue from the same animal. Ambra1 protein levels were monitored by western blot, using an anti Ambra1 antibody. **d)** p62 immunostaining on liver of *Ambra1* heterozygous (Ambra1$^{+/gt}$) mice. T: tumour. Scale bar, 100µm. **e)** Western blot analysis of p62 in liver of *Ambra1* heterozygous (*Ambra1*$^{+/gt}$) mice. Both tumour tissue and the surrounding healthy tissue were analysed from the same animal.
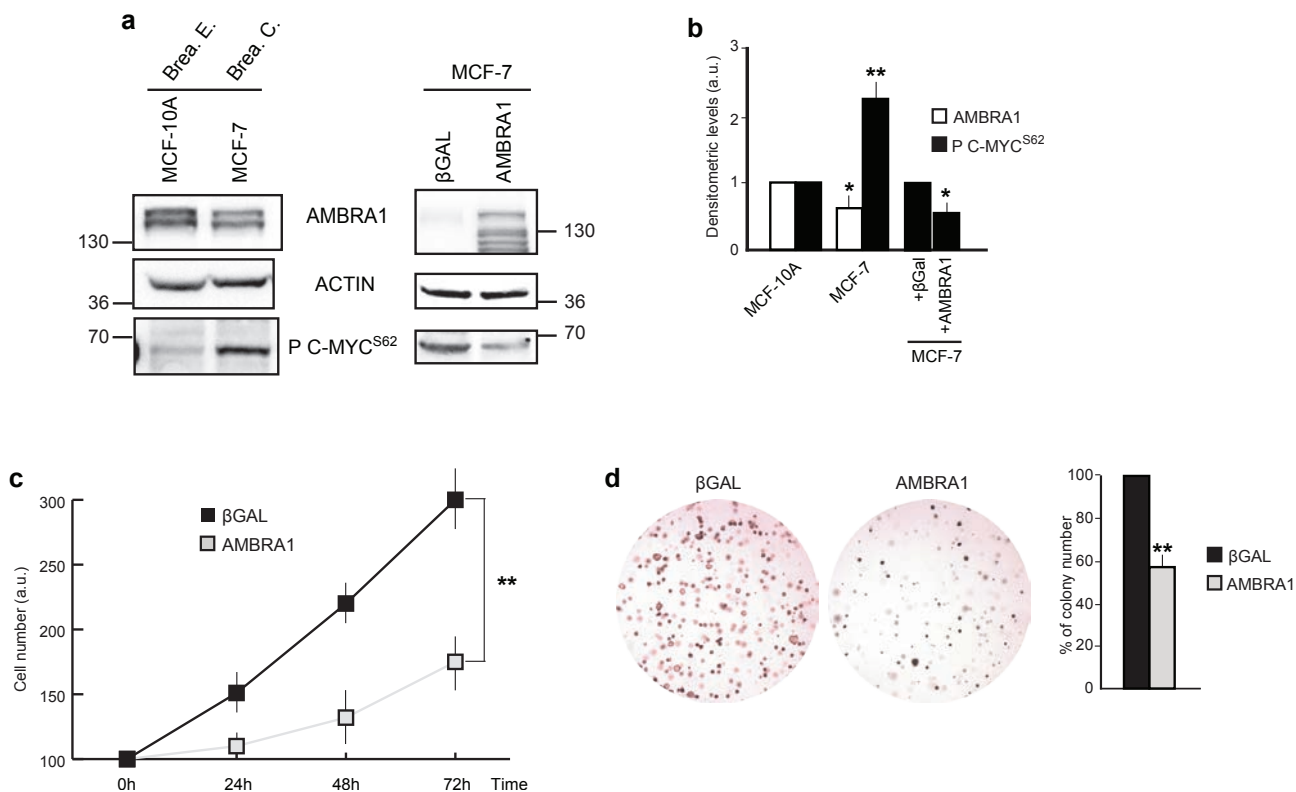
Supplementary Figure 6 Study of the functional correlation between AMBRA1 and P C-MYC^{S62} levels in MCF-7 **a)** Western blot analysis of AMBRA1 and P C-MYC^{S62} in human breast cell lines (MCF-10A cells, as a control, and the breast cancer derived cells, MCF-7). We observe an inverse correlation between AMBRA1 and P C-MYC^{S62} levels. On the right panel, MCF-7 cells were reconstituted for AMBRA1 and the levels of P C-MYC^{S62} were analysed by western blot. Brea. E.: Breast epithelium; Brea. C.: Breast cancer. **b)** Graph showing the correlation between AMBRA1 (white columns) and P C-MYC^{S62} (black columns) protein levels in lung cell lines analysed in **a**. Data are presented as means±s.d. and significance is *P< 0.05; **P<0.005 (n=6 independent experiments). **c)** MCF-7 cells, overexpressing AMBRA1 or βGal as control, by retroviral infection, were analysed by MTS assay at different time points. Data are presented as means±s.d. and significance is **P<0.005 (n=3 independent experiments). **d)** The tumorigenicity of the cells used in **c** was assessed by a colony formation assay in soft agar. Data are presented as means±s.d. and significance is **P<0.005 (n=4 independent experiments).
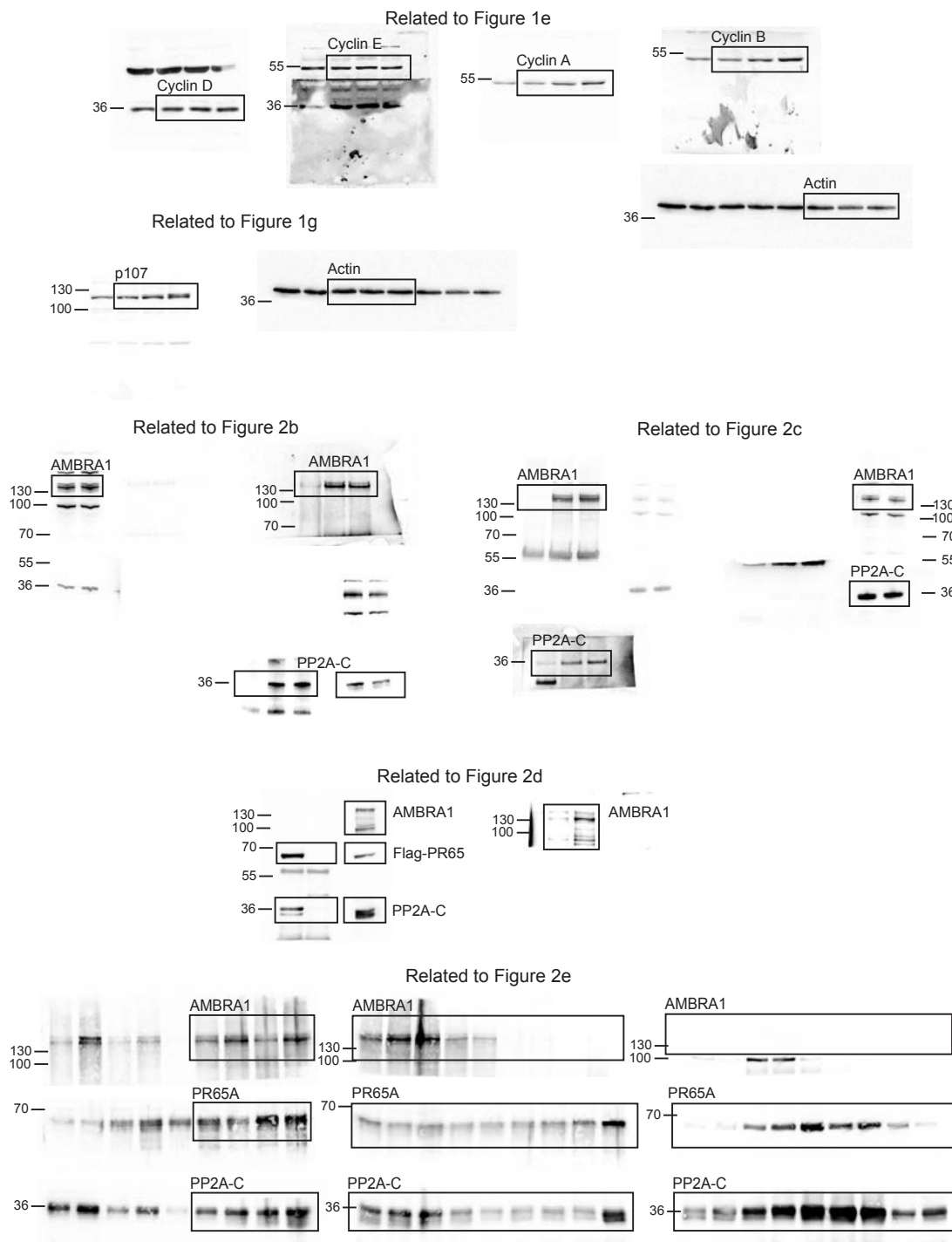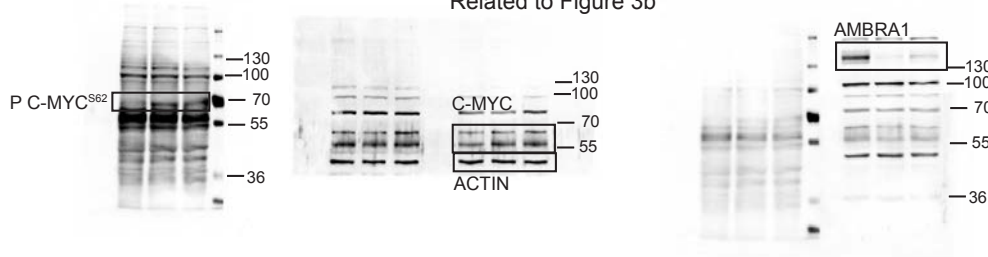
Supplementary Figure 7 Scans of Western Blot analyses Cropped regions are indicated by the boxes. Molecular weights are reported.
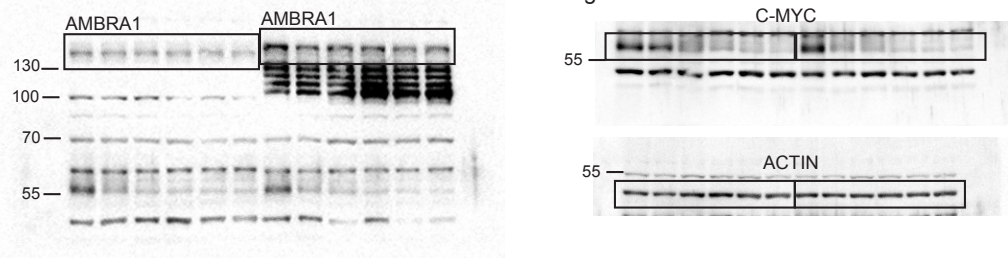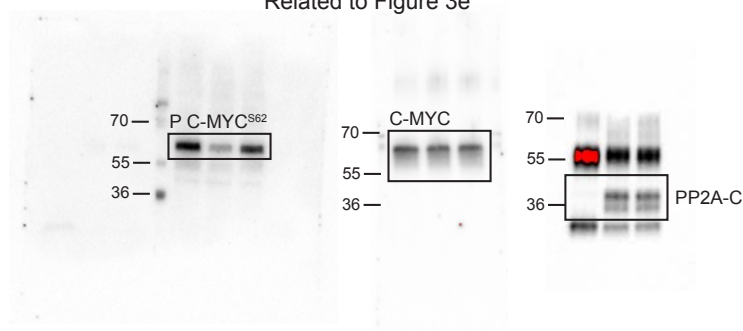
Related to Figure 3a
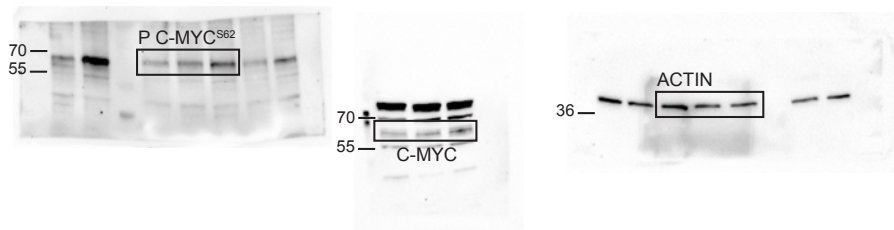
Related to Figure 3b
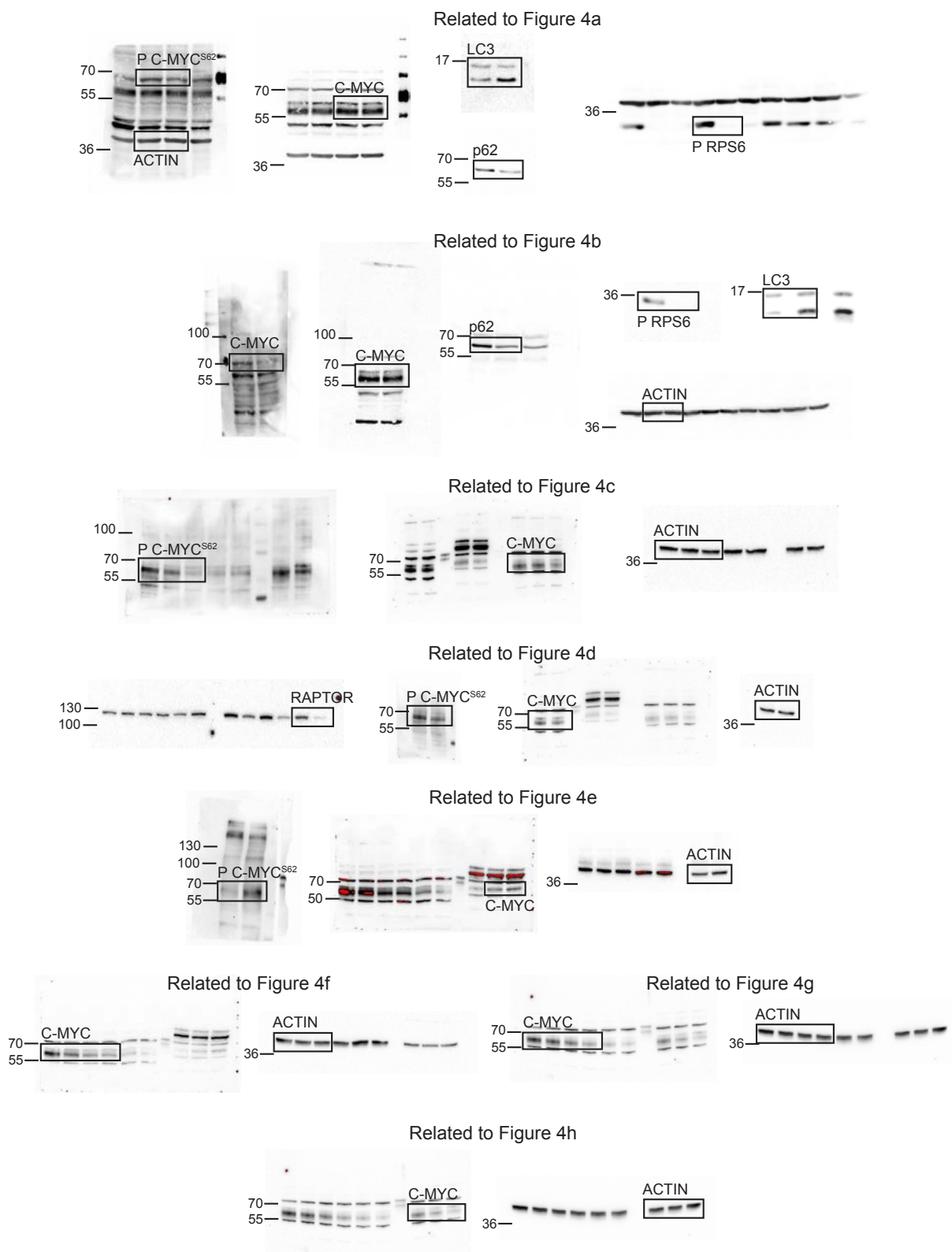

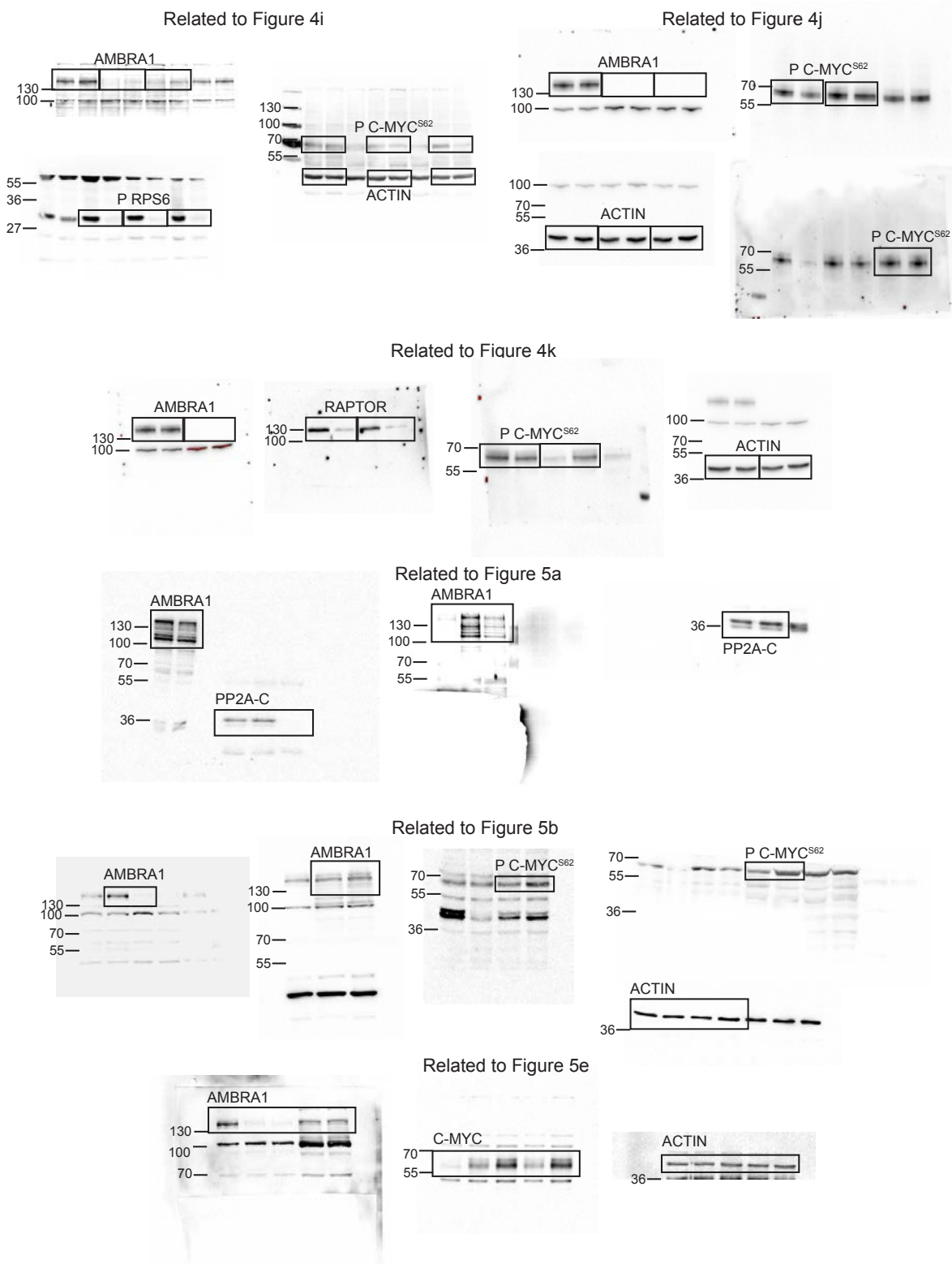Related to Figure 3d

Related to Figure 3e

Related to Figure 3f

Supplementary Figure 7 continued Scans of Western Blot analyses Cropped regions are indicated by the boxes. Molecular weights are reported.

Related to Figure 4a

Related to Figure 4b

Related to Figure 4c

Related to Figure 4d

Related to Figure 4e

Related to Figure 4f

Related to Figure 4g

Related to Figure 4h

Supplementary Figure 7 continued Scans of Western Blot analyses Cropped regions are indicated by the boxes. Molecular weights are reported.
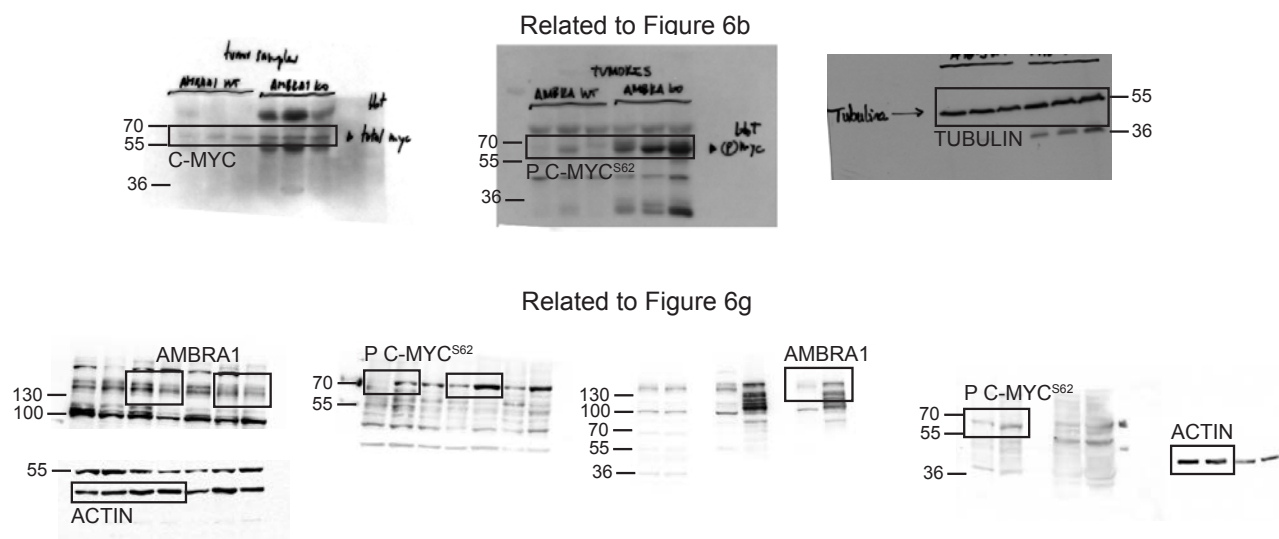
Supplementary Figure 7 continued Scans of Western Blot analyses Cropped regions are indicated by the boxes. Molecular weights are reported.

Related to Figure 6b

Related to Figure 6g

Supplementary Figure 7 continued Scans of Western Blot analyses Cropped regions are indicated by the boxes. Molecular weights are reported.

Supplementary Table 1 Protein quantification of PP2A-C (PPP2CB) and PR65A (PPP2R1A) interacting with AMBRA1, revealed by Tandem Affinity purification (TAP).[8] Proteins were grouped according to shared peptides. Following information is displayed in the respective columns. Proteins: number of proteins in the respective group; Peptides: number of peptides identified; Sequence coverage: amino acid sequence covered by identified peptides; PEP: posterior error probability; SILAC ratio: fold enrichment in AMBRA1 affinity purification; Ratio variability: standard deviation of the naturally logarithmized ratio times 100; Ratio count: redundant peptides used for quantification.